GEO-SEQ Project
Quarterly Status and Cost Report
September 1–November 30, 2002

Project Overview

The purpose of the GEO-SEQ Project is to establish a public-private R&D partnership that will:

- Lower the cost of geologic sequestration by: (1) developing innovative optimization methods for sequestration technologies with collateral economic benefits, such as enhanced oil recovery (EOR), enhanced gas recovery (EGR), and enhanced coalbed methane production; and (2) understanding and optimizing trade-offs between CO_2 separation and capture costs, compression and transportation costs, and geologic sequestration alternatives.
- Lower the risk of geologic sequestration by: (1) providing the information needed to select sites for safe and effective sequestration, (2) increasing confidence in the effectiveness and safety of sequestration by identifying and demonstrating cost-effective monitoring technologies, and (3) improving performance-assessment methods to predict and verify that long-term sequestration practices are safe, effective, and do not introduce any unintended environmental impact.
- Decrease the time to implementation by: (1) pursuing early opportunities for pilot tests with our private-sector partners and (2) gaining public acceptance.

In May 2000, a project kickoff meeting was held at Ernest Orlando Lawrence Berkeley National Laboratory (Berkeley Lab) to plan the technical work to be carried out, starting with FY00 funding allocations. Since then, work has been performed on four tasks: (A) development of sequestration co-optimization methods for EOR, depleted gas reservoirs, and brine formations; (B) evaluation and demonstration of monitoring technologies for verification, optimization, and safety; (C) enhancement and comparison of computer-simulation models for predicting, assessing, and optimizing geologic sequestration in brine, oil, and gas, and coalbed methane formations; and (D) improvement of the methodology and information available for capacity assessment of sequestration sites. Recently, a new task in support of the Frio Brine Pilot Project (E) has been added.

This Quarter's Highlights

- Numerous reactive-transport (open system) chemical-kinetic simulations, using reactive-transport codes, have been performed in support of the planning of the Frio Brine Pilot Project of south Texas. The simulation results are helpful in estimating water-chemistry evolution, mineral dissolution, and mineral growth as CO_2-rich aqueous fluids flow through the subsurface.

- A streamline-based proxy for full-reservoir simulation, allowing the rapid selection of a representative subset of stochastically generated reservoir models, has been investigated. Computationally intensive (and expensive) flow simulations should be performed using this type of subset.

- The applicability of the Advective Diffusive Model and the Dusty Gas Model to simulate transport in gas reservoirs with different permeabilities has been evaluated.

- Numerical calculations showed that injection of CO_2 into the Frio formation would produce an easily measurable streaming potential response. Modeling results also showed that a CO_2 wedge in a 10 m thick sand layer could be seismically detected. On the other hand, the associated gravity response might be too small for measurement.

- Modeling based on calculated pressure changes resulting from the injection of 5,000 tonnes of CO_2 indicates that tilt generated by deformation of the Frio B sand reservoir should be detectable using surface tiltmeters.

- Gas and isotope compositions in gases sampled at Lost Hills, California, in June 2002 indicate a substantial contribution of injected CO_2 in select wells compared to samples collected back in February 2002.

- In anticipation of the Frio Brine Pilot Project CO_2 injection tests, detailed experiments have been conducted on perfluorocarbon tracer gas chromatography analytical methods, their reproducibility, and sensitivity. Preliminary gas chemistry and isotope analysis of the CO_2 manufactured by the plant that will supply the gas to used in the project were also conducted.

- The comparison of different reservoir simulation codes used in the modeling of CO_2 injection into geologic formations continued. The results of the intercomparisons have been documented.

- Additional modeling studies of the Frio Brine Pilot Project CO_2 injection experiment were performed, focusing on the impact of the characteristic curves used (in particular, the assumed value of the residual gas saturation).

- The preparation of permits for the Frio Brine Pilot Project is near completion. More detailed plans have been developed to integrate the various GEO-SEQ experiments with the project's well design and test schedule.

Papers Presented, Submitted, Accepted, or Published during This Quarter

Benson, S.M. et al., The GEO-SEQ Project: A status report. Paper presented at the Sixth International Conference on Greenhouse Gas Technologies (GHGT-6), Kyoto, Japan, October 1–4, 2002.

Boram, L.H., S.R. Higgins, K.G. Knauss, and C.M. Eggleston, Plagioclase dissolution and carbonate growth related to CO_2 sequestration in deep aquifers: EQ3/6 modeling and laboratory experiments. Paper presented at the 2002 GSA Annual Meeting and Exposition, Denver, Colorado, October 27–30, 2002.

Cole, D. R., The influence of nanoscale porosity on structure and dynamics of fluids. Paper presented at the 2002 GSA Annual Meeting and Exposition, Denver, Colorado, October 27–30, 2002.

Doughty, C., S.M. Benson, and K. Pruess, Capacity investigation of brine bearing sands for geologic sequestration of CO_2. Poster presented at the Sixth International Conference on Greenhouse Gas Technologies (GHGT-6), Kyoto, Japan, October 1–4, 2002.

Gunter, W.D., and D.H.-S. Law, Enhanced coalbed methane recovery and CO_2 storage: Simulation issues and model comparison. Paper presented at the International Workshop on the "Present Status and Outlook of CO_2 Sequestration in Coal Seams," Tokyo, Japan, September 5, 2002.

Hoversten, G.M., Non-seismic geophysics for CO_2 sequestration monitoring. Paper presented at the 2002 Society of Exploration Geophysicists Workshop on CO_2 Sequestration, Salt Lake City, UT, October 10, 2002.

Hoversten, G.M., R. Gritto, T.M. Daley, E.L. Majer, and L.R. Myer, Crosswell seismic and electromagnetic monitoring of CO_2 sequestration. Paper presented at the Sixth International Conference on Greenhouse Gas Technologies (GHGT-6), Kyoto, Japan, October 1-4, 2002.

Hovorka, S.D., and P.R. Knox, Frio Brine sequestration pilot in the Texas Gulf Coast. Paper presented at the Sixth International Conference on Greenhouse Gas Technologies (GHGT-6), Kyoto, Japan, October 1–4, 2002.

Johnson, J.W. et al., CO_2 floods for co-optimized EOR and sequestration: Technology development and demonstration. Paper presented at the Sixth International Conference on Greenhouse Gas Technologies (GHGT-6), Kyoto, Japan, October 1–4, 2002.

Johnson, J.W., and J.J. Nitao, Reactive transport modeling of geologic CO_2 sequestration at Sleipner. Paper presented at the Sixth International Conference on Greenhouse Gas Technologies (GHGT-6), Kyoto, Japan, October 1–4, 2002.

Johnson, J.W., J.J. Nitao, C.I. Steefe, and K. G. Knauss, Reactive transport modeling of geologic CO_2 sequestration. Paper presented at the 2002 GSA Annual Meeting and Exposition, Denver, Colorado, October 27–30, 2002.

Knauss, K.G., J.W. Johnson, and L.H. Boram, Impact of CO_2, contaminant gas, aqueous fluid, and reservoir rock interactions on the geologic sequestration of CO_2. Paper presented at the 2002 GSA Annual Meeting and Exposition, Denver, Colorado, October 27–30, 2002.

Knox, P.R., S.D. Hovorka, and C.M. Oldenburg, Potential new uses for old gas fields: sequestration of carbon dioxide, Gulf Coast Association of Geological Societies and Gulf Coast Section SEPM Transactions, 52, 563–571.

Law, D.H.-S, L.H.G. van der Meer, and W.D. Gunter, Comparison of numerical simulators for greenhouse gas storage in coalbeds, Part II: Flue gas injection. Paper presented at the Sixth International Conference on Greenhouse Gas Technologies (GHGT-6), Kyoto, Japan, October 1–4, 2002.

Law, D.H.-S, L.H.G. van der Meer, P. Sammon, L. Pekot, and W.D. Gunter, New development on coalbed methane simulators for enhanced coalbed methane recovery processes. Paper presented at the Geological Society of America Annual Meeting, Denver, Colorado, October 27–30, 2002 .

Myer, L.R., G.M. Hoversten, and C.A. Doughty, Sensitivity and cost of monitoring geologic sequestration using geophysics. Poster presented at the Sixth International Conference on Greenhouse Gas Technologies (GHGT-6), Kyoto, Japan, October 1–4, 2002.

Newmark, R., A. Ramirez, and W. Daily, Monitoring carbon dioxide sequestration using electrical resistance tomography (ERT): a minimally invasive method. Paper presented at the Sixth International Conference on Greenhouse Gas Technologies (GHGT-6), Kyoto, Japan, October 1–4, 2002.

Oldenburg, C.M., Carbon dioxide as cushion gas for natural gas storage. Paper to appear in Energy & Fuels, 2003.

Oldenburg, C.M., D.H.-S. Law, Y. Le Gallo, and S.P. 2002, White, Mixing of CO_2 and CH_4 in gas reservoirs: Code comparison studies. Paper presented at the Sixth International Conference on Greenhouse Gas Technologies (GHGT-6), Kyoto, Japan, October 1–4, 2002.

Oldenburg, C.M., S.H. Stevens, and S.M. Benson, Economic feasibility of carbon sequestration with enhanced gas recovery (CSEGR). Paper presented at the Sixth International Conference on Greenhouse Gas Technologies (GHGT-6), Kyoto, Japan, October 1–4, 2002.

Oldenburg, C.M., S.W. Webb, K. Pruess, and G.J. Moridis, Mixing of stably stratified gases in subsurface reservoirs: A comparison of diffusion models. Paper submitted to Transport in Porous Media, 2002.

Pruess, K., A. Bielinski, J. Ennis-King, R. Fabriol, Y. Le Gallo, J. García, K. Jessen, T. Kovscek, D. H.-S. Law, P. Lichtner, C. Oldenburg, R. Pawar, J. Rutqvist, C. Steefel, B. Travis, C.F. Tsang, S. White, and T. Xu, Code intercomparison builds confidence in numerical models for geologic disposal of CO_2. Paper presented at the Sixth International Conference on Greenhouse Gas Technologies (GHGT-6), Kyoto, Japan, October 1–4, 2002.

Pruess, K. and J. García, Solutions of test problems for disposal of CO_2 in saline aquifers. Lawrence Berkeley National Laboratory Report LBNL-51812, November 2002.

Pruess, K., J. García, T. Kovscek, C. Oldenburg, J. Rutqvist, C. Steefel and T. Xu, Intercomparison of numerical simulation codes for geologic disposal of CO_2. Lawrence Berkeley National Laboratory Report LBNL-51813, November 2002.

Pruess, K., T. Xu, J. Apps and J. García, Numerical modeling of aquifer disposal of CO_2. Paper SPE-6653, to appear in Society of Petroleum Engineers Journal, 2003.

Rau, G.H., K. Caldeira, and K. Knauss, A geochemical solution to the atmospheric CO_2 problem? Paper presented at the 2002 GSA Annual Meeting and Exposition, Denver, Colorado, October 27–30, 2002.

Task Summaries

Task A: Develop Sequestration Co-Optimization Methods

Subtask A-1: Co-Optimization of Carbon Sequestration, EOR, and EGR from Oil Reservoirs

Goals

To assess the possibilities for co-optimization of CO_2 sequestration and enhanced oil recovery (EOR), and to develop techniques for selecting the optimum gas composition for injection. Results will lay the groundwork necessary for rapidly evaluating the performance of candidate sequestration sites, as well as monitoring the performance of CO_2 EOR.

Previous Main Achievements

- Screening criteria for selection of oil reservoirs that would co-optimize EOR and maximize CO_2 storage in a reservoir have been generated.

Accomplishments This Quarter

- A streamline-based proxy for full reservoir simulation has been investigated thoroughly. It allows a modeler to rapidly select a representative subset of stochastically generated reservoir models that encompasses uncertainty with respect to true reservoir geology. It is upon this subset that computationally expensive flow simulations should be conducted.

Progress This Quarter

We have developed a synthetic 3-D model of an oil reservoir that includes a realistic reservoir fluid description. The description of heterogeneities and their distribution is geostatistical, in that multiple reservoir models can be generated capturing some sense of variability and uncertainty. This is typical of oil reservoir characterization. The properties of unit-mobility ratio streamlines are well suited to probe the range of possible flow behaviors. For example, **Figure 1** illustrates the direct correlation among streamline results and full reservoir simulation for CO_2 injection into the reservoir model. Each symbol represents the results from a stochastic realization of a reservoir model. Fully compositional results are plotted on the y-axis, and unit mobility ratio streamline

results are plotted on the x-axis. **Figure 1(a)** plots the difference between the results of a reference or "true" reservoir model and various equiprobable realizations. The quantity considered for this comparison is the fraction of the injected CO_2 that is produced after 5,000 days. While there is scatter among the results, the streamline and the fully compositional results clearly correlate. **Figure 1(b)** plots the storage of CO_2 relative to the volume injected for each model. Results here correlate strongly with a correlation coefficient of 0.89.

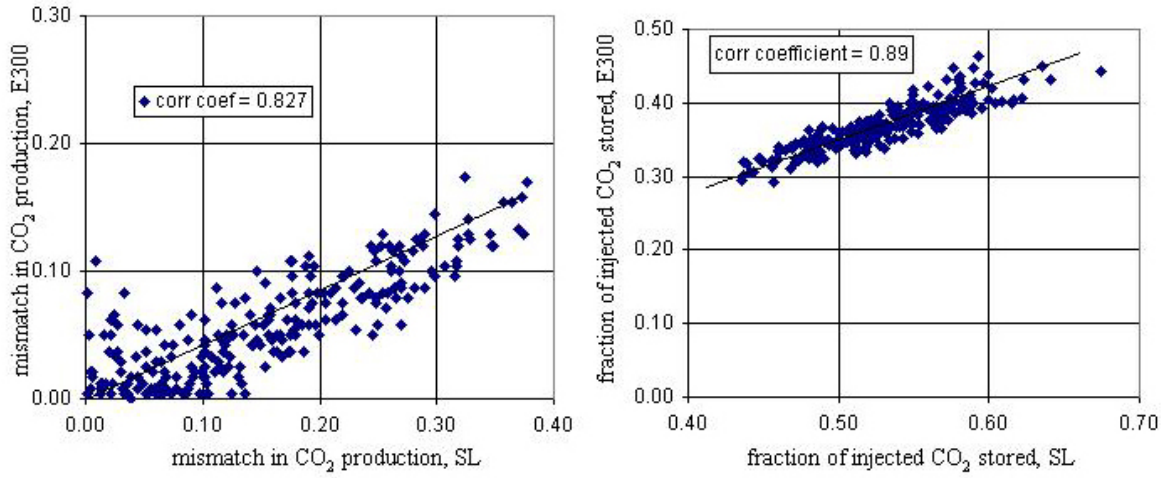

Figure 1. Correlation among Eclipse 300 (E300) fully-compositional simulations and unit-mobility ratio streamline (SL) calculations (injection gas is pure CO_2.): (a) the difference or "mismatch" in simulation results between and a realization and the reference or "true" model, with the quantity considered being the fraction of cumulative injected CO_2 produced at 5,000 days; (b) the fraction of injected CO_2 retained or stored within the reservoir.

The implications are that a modeler can reduce significantly the number of full-physics reservoir simulations needed to fully characterize the variability expected at a particular site. A subset of models that span the range of possible behaviors are easily identified. Furthermore, simplified calculations such as these streamline computations can be used in a first pass to decide optimal placement of wells and how those wells should be completed (e.g., fully completed or partially completed over the reservoir interval).

A common problem with gas injection is the high mobility of CO_2 compared to the resident fluids. Adverse mobility ratios lead to premature breakthrough of CO_2 at production wells and incomplete sweep of reservoir volume. Aqueous foams have the ability to profoundly alter the mobility of injected gas. To this end, we have designed and constructed an experimental apparatus that will be used to measure the trapping of CO_2 by foam. Experiments have been designed so that X-ray CT scanning can monitor the progress of CO_2 injection into a sandstone.

Work Next Quarter

The streamline proxy results, such as shown in **Figure 1**, will be written up as a paper to be submitted to a journal. In addition, our work continues on considering, via reservoir simulation, various reservoir development scenarios to understand better reservoir development techniques that maximize the simultaneous production of oil and storage of CO_2. These scenarios are being evaluated using the reservoir models chosen above. We are examining (in order): water-alternating-gas (WAG) drive mode, CO_2 injection early in production life versus late in reservoir life, CO_2 injection following waterflooding, and stripping of CO_2 from a mixture of CO_2 and N_2 to simulate an incompletely separated combustion gas.

The experimental effort on CO_2 trapping by foam will continue. We expect to conduct a number of experiments in the next quarter. The *in situ* distribution of CO_2 will be imaged using X-ray computed tomography.

Subtask A-2: Feasibility Assessment of Carbon Sequestration with Enhanced Gas Recovery (CSEGR) in Depleted Gas Reservoirs

Goals

To assess the feasibility of injecting CO_2 into depleted natural gas reservoirs for sequestering carbon and enhancing methane (CH_4) recovery. Investigation will include assessments of (1) CO_2 and CH_4 flow and transport processes, (2) injection strategies that retard mixing, (3) novel approaches to inhibit mixing, and (4) identification of candidate sites for a pilot study.

Previous Main Achievements

- On the basis of numerical-simulation studies, the proof-of-concept for CO_2 storage with enhanced gas recovery (CSEGR) was demonstrated.

Accomplishments This Quarter

- It was concluded that the Advective Diffusive Model (ADM) is adequate for simulating transport in high-permeability gas reservoirs, while the Dusty Gas Model (DGM) is more appropriate for lower permeability units.

Progress This Quarter

At the Kyoto GHGT-6 conference, Curt Oldenburg presented his work on (1) code intercomparison related to gas reservoir sequestration and (2) economic analyses of CSEGR. In addition, he prepared and submitted a manuscript showing comparisons of the ADM and DGM for gas reservoir mixing to the journal *Transport in Porous Media*. The purpose of this latter comparison study is to determine under what conditions the computationally cheaper ADM can be used instead of the more rigorous but more expensive DGM. The model problem consists of a one-dimensional gas reservoir initially at 40 bars and 40ºC with a layer of CO_2 below a layer of CH_4. Mixing occurs at the interface between these stably stratified gases, mostly by diffusion. **Figure 2** shows the pressure and gas mole fractions of CO_2 and CH_4 for the ADM and DGM over time, for permeability equal to 10^{-15} m^2 and 10^{-18} m^2. As shown, the ADM and DGM agree closely for k = 10^{-15} m^2, whereas they deviate for k = 10^{-18} m^2. We have concluded from this study that the ADM is adequate for high permeability gas reservoirs, and that the DGM should be used for simulating transport in low permeability units such as caprock.

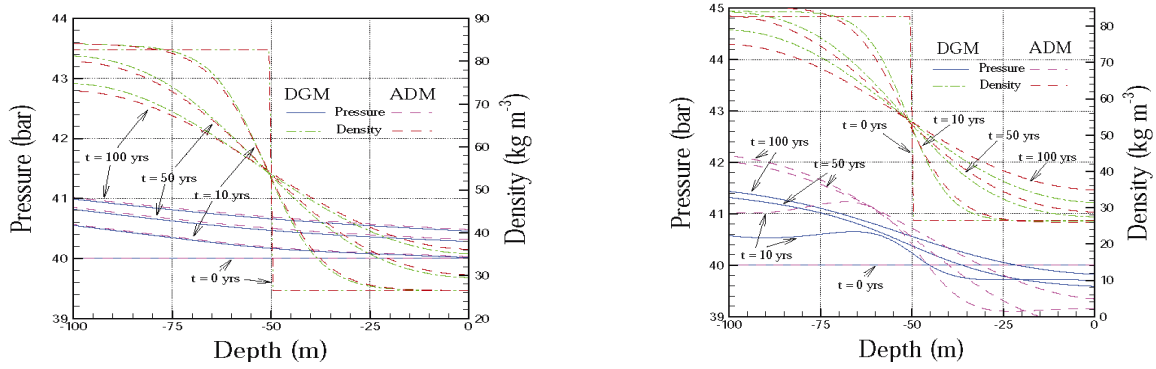

Figure 2. Vertical profiles of pressure and gas-phase density for mixing with permeability equal to 10^{-15} m^2 (left) and 10^{-18} m^2 (right).

Work Next Quarter

- We will add and test an improved solubility model for TOUGH2/EOS7C.
- We will work with subcontractor Scott Stevens to finish economic feasibility assessment work for additional regions in the U.S.
- We will continue to work with Paul Knox to identify a potential CSEGR pilot site.

Subtask A-3: Evaluation of the Impact of CO_2 Aqueous Fluid and Reservoir Rock Interactions on the Geologic Sequestration of CO_2, with Special Emphasis on Economic Implications.

Goals

To evaluate the impact on geologic sequestration of injecting an impure CO_2 waste stream into the storage formation. By reducing the costs of the front-end processes, the overall costs of sequestration could be dramatically lowered. One approach is to sequester non-pure CO_2 waste streams that are less expensive or require less energy than separating pure CO_2 from the flue gas.

Previous Main Achievements

- Potential reaction products have been determined based upon reaction-progress chemical thermodynamic/kinetic calculations for typical sandstone and carbonate reservoirs into which an impure CO_2 waste stream is injected.
- Reactive-transport simulations have been completed for a plug-flow reactor (PFR) run to be made using the Frio Formation core material acquired in support of Task E.

Accomplishments This Quarter

- Using TOUGH2 results from Chris Doughty (LBNL) as a starting point for hydrological conditions, we have made numerous reactive-transport (open system) chemical-kinetic simulations using the reactive-transport simulator CRUNCH (Steefel, 2001). These new simulations were made in support of planning for the Frio Pilot Project in Texas (Task E). They use cylindrical coordinates and a 1-D approximation for the radial flow field that Doughty calculated in her TOUGH2 simulations, which allowed us to match her arrival times at the observation well. We can then approximate water-chemistry evolution and mineral dissolution and growth in response to the flow of a CO_2-rich aqueous fluid.
- New pump operating software was installed on the Quizix pump that controls flow in our plug-flow reactor. This was required in order to be able to supply a pressurized (CO_2-charged) fluid as input to the pump. Confirmatory reactive-transport experiments, intended to lend credibility to the model calculations and simulations done to date and planned for the future, will begin in December 2002.

Progress This Quarter

During this quarter, we continued the process of evaluating the impact of waste-stream CO_2, as well as contaminants (e.g., SO_2, NO_2 and H_2S), on injectivity and sequestration performance.

Our current goal is to try to predict chemical and mineralogical changes that we might expect to see in a one-year Frio Pilot Project (Task E), consisting of a 15-day injection period, followed by 11.5 months of postinjection observation. This new scenario (a shorter injection period) reflects the decreased CO_2 available, owing to the additional costs associated with drilling a new (closer) injection well. These simulation results will be helpful in obtaining permits to conduct the field test.

In recent TOUGH2 simulations of CO_2 injection into the "C" sand (250 T/d), Chris Doughty (LBNL) found that after approximately 5 days, the effects of the advancing CO_2 plume should be observable at the observation well, 30 meters away from the new injection well. We used an analytical expression to calculate a radial Darcy flow field that closely approximates the flow field that results from the TOUGH2 modeling. We used the same downhole temperature (64°C) and total pressure (150b CO_2) as was used in the TOUGH2 simulation. This results in a CO_2 fugacity of 84.3 b. We also used the same sand porosity of 30%.

We set the problem up as a very simple 1-D simulation, which approximates a single streamline between the injection well and the observation or production well. We further simplified transport by only considering flow of a single (liquid) CO_2-rich aqueous phase, because in the field we will be acquiring primarily liquid aqueous samples (including dissolved gases) at any observation well. We injected the aqueous fluid for 15 days at the rate calculated for the first cell in the radial flow field and ran CRUNCH using cylindrical coordinates, applying the calculated radial flow field across the domain. As will be shown below, this results in a front arrival time at the observation well that is similar to that calculated by TOUGH2. In the simulation, we used a domain that extended 300 m beyond the observation well. After the 15-day injection period, we instantaneously switched to a constant, linear flow field at a low rate (Darcy flow of 0.15 m/y) to approximate the return of background regional flow. Note that the simulations contained in the last quarterly report used a constant linear flow field and had an observation well located 135 m away from the injection well, which corresponds to the situation for the existing wells at South Liberty.

In our simulation the mineralogy of the Frio Fm. "C" sand was assumed to be that found at a stratigraphically equivalent depth for hole Merisol WDW No. 319. The modal abundances and compositions were determined using XRD in a report provided by Dan Collins (SandiaTech). The starting mineralogy consisted of the appropriate mix of quartz, K-feldspar, plagioclase (compositionally An60 with thermodynamic properties calculated as an ideal mixture of end-member albite and anorthite), pyrite, muscovite (as a proxy for illite), kaolinite, clinochlore (as the Mg end-member chlorite) and calcite as the cement mineral. Because the formation fluid becomes very acidic near the injection well (pH 3.3), we use full-kinetic rate laws for each mineral, accounting for acid catalysis. The chemical elements comprising the model formation fluid were based on compositions for Frio Fm waters taken from well GNI WDW-169, and included Ca, Mg, Ba, Sr, Na, Cl, S, Fe, C, Al, Si, and H. Preliminary equilibrium modeling required to speciate the model water at run initialization suggested that possible secondary minerals included barite, chalcedony, dawsonite, magnesite, siderite, and strontianite. These minerals could precipitate, as well as any of the primary minerals, and kinetic rate laws also governed precipitation.

As examples of the results obtained in the recent simulations, we show in **Figure 3** the breakthrough curves at the observation well (i.e., the solution concentrations at the observation well as a function of time) for elements of potential interest. The top curves are identical to the corresponding bottom curves, but with expanded time scales to make arrival time at the observation well more obvious. Note that the tracer-front midpoint arrives at the observation well in approximately 5 days. The tracer is a fictive, perfectly conservative element that travels with the velocity of the fluid. The 15-day injection period is equivalent to 0.04 years.

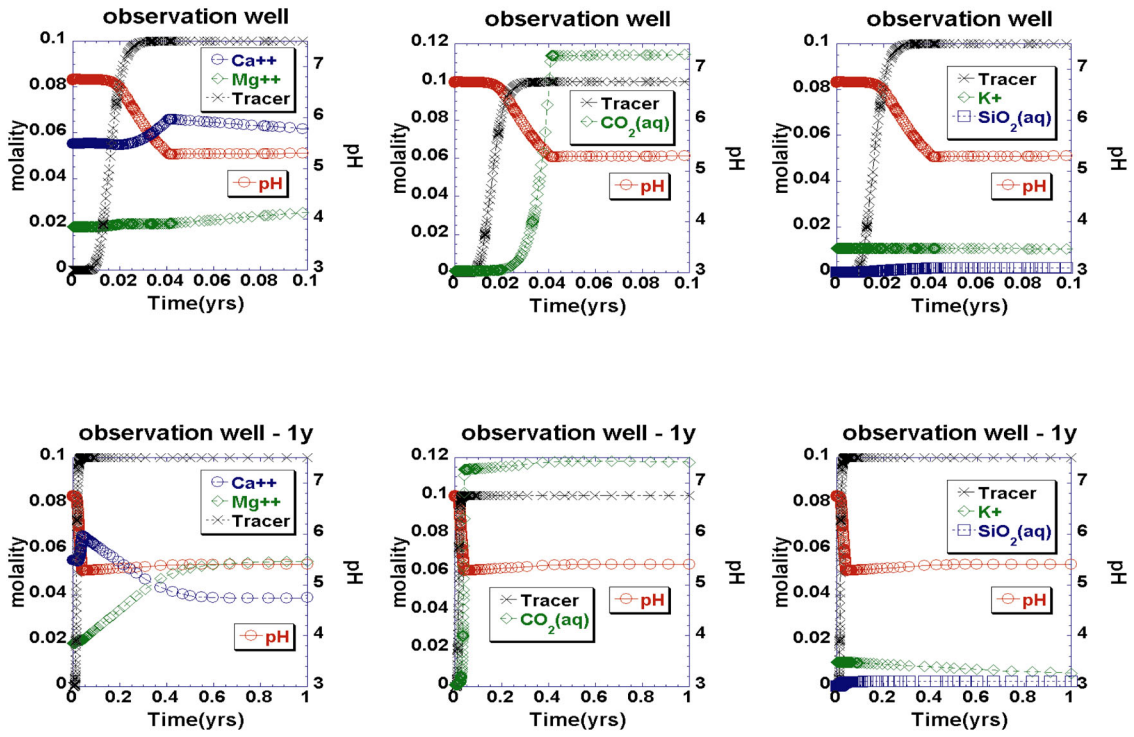

Figure 3. Breakthrough curves at the observation well

The primary impact of injecting CO_2 is to drive the pH down, buffered by the calcite cement, although the cement is completely consumed near the well bore (see **Figure 4**), where the pH drops to that fixed by saturation with respect to 84.3b of CO_2. The low pH, especially near the injection well, destabilizes many of the primary minerals, and they dissolve, increasing the fluid concentrations of Ca (from calcite and anorthite), Mg (from clinochlore), and to a lesser extent K (from K-feldspar) and Si (from all of the silicates). Although not plotted owing to the scale, Al also increases in concentration, resulting from the dissolution of aluminosilicates (primarily K-feldspar). After the injection period, at the location of the observation well, the Ca decreases due to the formation of calcite.

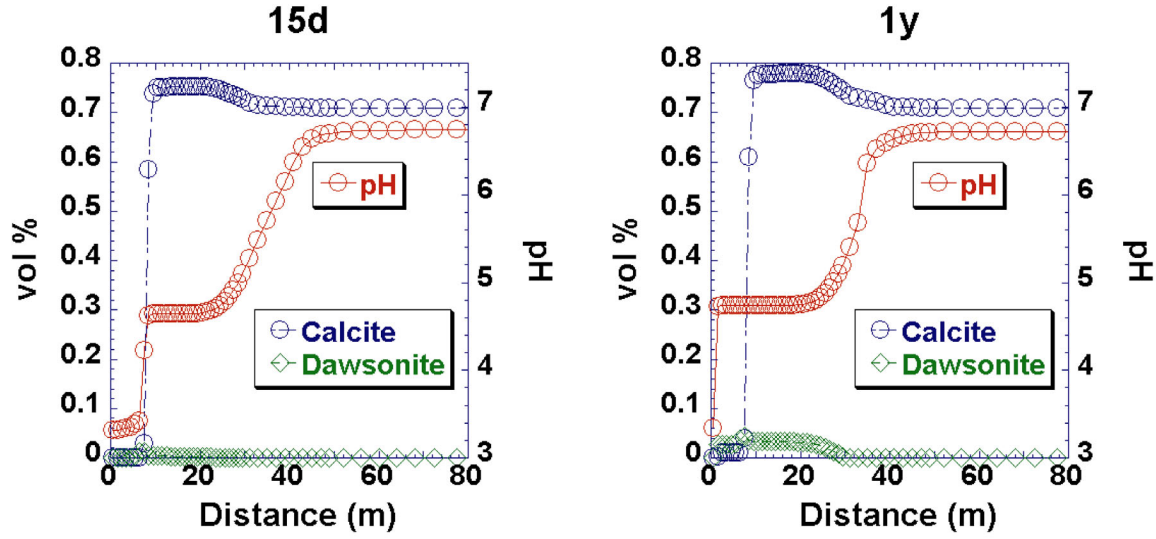

Figure 4. Carbonate mineral distribution away from injection well

The simulation also predicts the formation of several carbonate minerals along the flow path in locations in space and time primarily dictated by the fluid pH. **Figure 4** shows that dawsonite and calcite are predicted to form and, although not plotted, magnesite is also predicted to form. Although some of the carbonate (calcite) predicted to grow simply represents mobilized carbonate cement, the bulk of it represents CO_2 carbon being sequestered by mineral trapping. However, in terms of total mass over this short time period, the mass of carbon sequestered by solubility in the aqueous phase dwarfs that sequestered by carbonate mineral precipitation.

These simulations, although hydrologically simple, illustrate the types of chemical and mineralogical changes that we might expect resulting from CO_2 injection into a Frio-type setting. The chemical signal produced in the water advancing just ahead of the CO_2 front should be easily measurable, assuming the front is radial and actually reaches the observation well (i.e., the observation well is directly up-dip).

Work Next Quarter

We will continue investigating the impact of CO_2, as well as other contaminants (SO_2, H_2S, NO_2, etc.) in the CO_2 waste stream. Our attention will become more focused on work that may help in the design and conduct of the Frio Pilot Project (Task E). In particular, we plan to begin reactive transport experiments, reacting Frio "C" sand equivalent material with NaCl solutions equilibrated with appropriate CO_2 fugacities, using a specially modified plug-flow reactor. These experiments will provide our first real test of the simulations that have been done to date.

Task B: Evaluate and Demonstrate Monitoring Technologies

Subtask B-1: Sensitivity Modeling and Optimization of Geophysical Monitoring Technologies

Goals

To (1) demonstrate methodologies for, and carry out an assessment of, the effectiveness of candidate geophysical monitoring techniques; (2) provide and demonstrate a methodology for designing an optimum monitoring system; and (3) provide and demonstrate methodologies for interpreting geophysical and reservoir data to obtain high-resolution reservoir images. The Chevron CO_2 pilot at Lost Hills, California, has been used as an initial test case for developing these methodologies.

Previous Main Achievements

A methodology for site-specific selection of monitoring technologies was established and demonstrated.

Modeling studies based on well logs from the Liberty Field in south Texas showed that before CO_2 injection, seismic reflection from shale-sand interfaces decreases in amplitude with increasing depth. As CO_2 is injected at shallow depth, reflectivity sharply decreases.

The studies also indicated that even if a CO_2 wedge were seismically detected because of geometric effects, interpretation of the reflection for fluid properties would be difficult until the horizontal extent of the CO_2 zone exceeds one seismic Fresnel zone.

Accomplishments This Quarter

Numerical simulation results show that injection of CO_2 into the Liberty Field (south Texas) formation would produce a streaming potential (SP) response that is easily measured. For the Sleipner CO_2 injection tests, the results are less encouraging. However, a number of key parameters are poorly defined, and definitive statements about the potential of SP as a monitoring tool cannot yet be made.

Modeling studies were performed to calculate contrasts in seismic velocity, density and impedance when CO_2 is injected into a brine-saturated rock. Results for geology appropriate for the Liberty Field showed that a wedge of CO_2 in a 10 m thick sand layer could be seismically detected. The gravity response was much less sensitive. The smallest volume that could be detected at 1,000 m depth was equivalent to 20 days production from a 1,000 MW coal-fueled power plant.

Progress This Quarter

Self-potential method

We have tested and verified a streaming potential (SP) numerical simulation code developed by Sill (1983). The details of the SP response were described in the June–August 2000 report. The key equation describing the important parameters in the SP response is:

$$L\frac{\Gamma\mu}{k\sigma} = \nabla\phi \qquad (1)$$

In Equation (1), L is the coupling coefficient between flow and electric potential, Γ is the fluid flux, μ is the fluid viscosity, k is the magnetic permeability of the rock-fluid mix, σ is the electric conductivity of the rock-fluid mix, and ϕ is the electric potential. The key parameter L, the coupling coefficient, has only been measured for a very few fluids, as reported in the literature. In general, the more resistive the fluid, the larger L is. We have used a value reported for benzene as a proxy for CO_2. While the value for CO_2 will undoubtedly be different, its magnitude should be comparable. The determination of L for CO_2 flowing in brine-saturated sandstone is a major unknown to be determined in the coming quarter by experiment at LBNL.

Given the limited information we have on coupling coefficients, our results are very preliminary. However, those results suggest that further work on quantifying the SP response of CO_2 injection is worth pursuing.

We have built a 2-D numerical model based on the geology and configuration of the Liberty Field CO_2 injection test (Task E). The model consists of a 10 m thick sand layer at a depth of 1,500 m embedded in shale. The resistivity of the sand unit is 2 Ohm-m, while the resistivity of the surrounding shale is 1 Ohm-m. The CO_2 has a flow rate of 350 kg/s, a viscosity of CO_2 73 μPa-s, and a density of 788 kg/m^3 (at a temperature of 70° C and a pressure of 30 MPa). The model is shown in **Figure 5.**

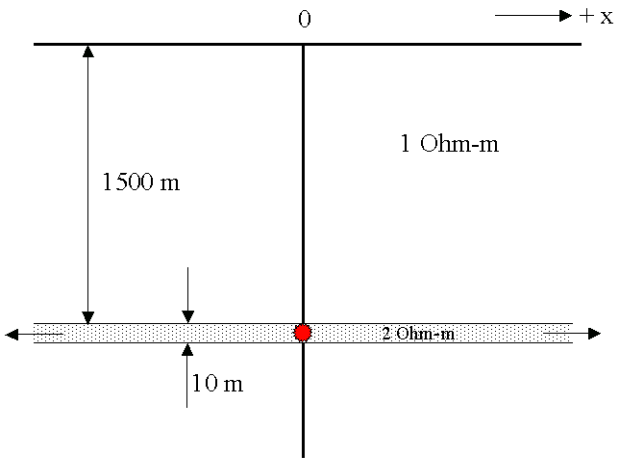

Figure 5. Model simulating the Liberty Field geology; 10 m thick sand layer at the depth of 1500 m.

Figure 6 shows a pressure distribution for this model. **Figure 7** is the electric potential cross-section for the same model. In general, SP noise sources are on the order of a few to 10s of mV, although this number is highly site specific. Signals over 10 mV are considered to be large.

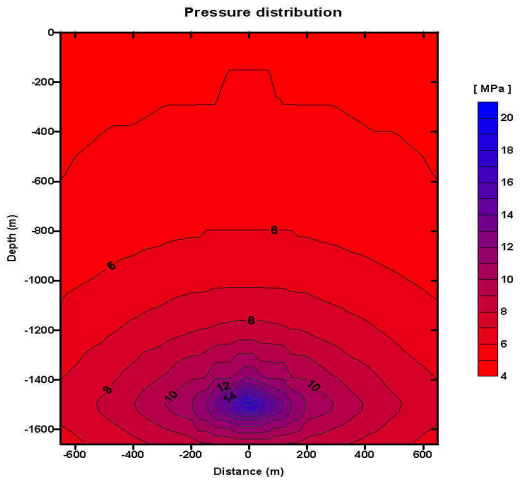

Figure 6. Pressure distribution for the model from **Figure 5**

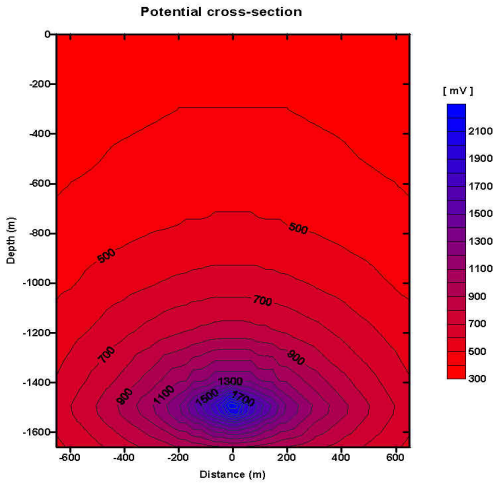

Figure 7. Potential cross section for the model from **Figure 5**

We were interested not only in the surface SP and pressure responses for the model described above, but also in a sensitivity of the method to the CO_2 extend. Therefore, we created a model with the same parameters as the previous model, except that the sand layer was terminated at +300 m. The model is shown in **Figure 8**. The surface pressure response is shown in **Figure 9**, while the SP response is shown in **Figure 10**.

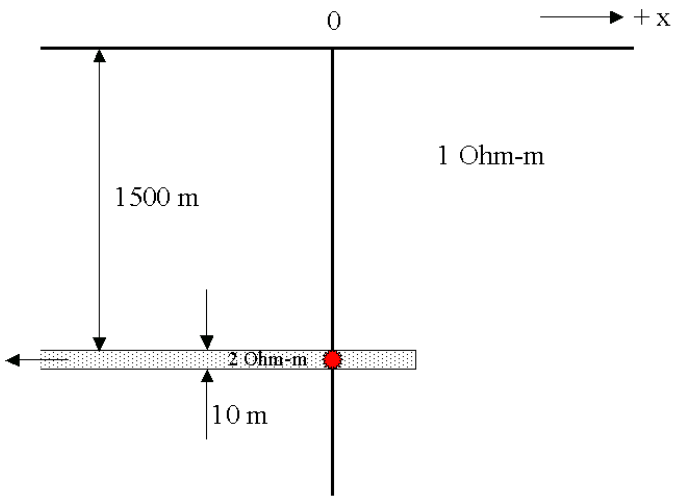

Figure 8. Model simulating the Liberty Field geology; 10 m thick sand layer at the depth of 1,500 m truncated at +300 m

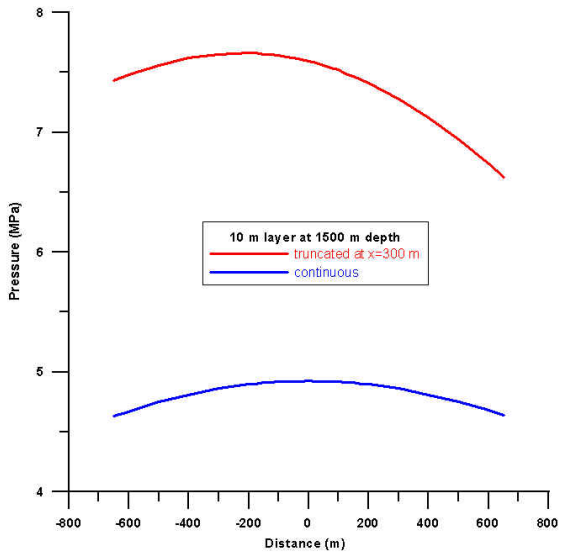

Figure 9. Surface pressure response for the model from **Figure 8**

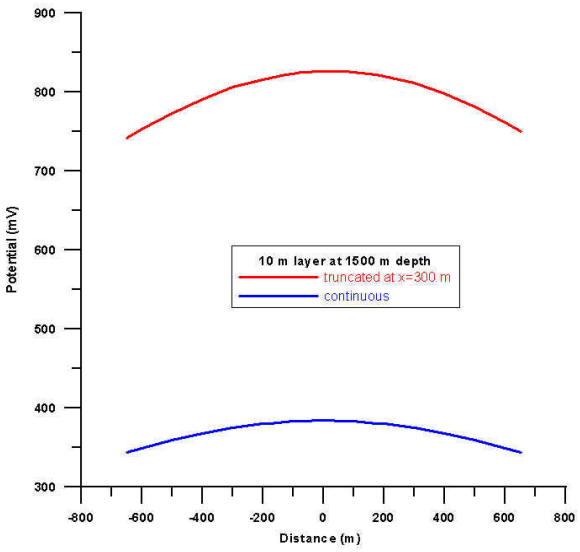

Figure 10. SP response for the model from **Figure 8**

We can see an asymmetric pressure response and the increase in the electric potential response due to the truncation of the layer. This result indicates that information exists in the SP surface response about the spatial distribution of CO_2 at depth. If further investigation of the SP coupling coefficients indicates that our numerical models are valid, we will consider development of an inverse algorithm to access the ability to image the spatial distribution of CO_2 from the surface SP data.

We have also investigated amplitude of the surface SP response with respect to the depth of the sand layer. **Figure 11** shows SP response for a 100 m thick sand layer at 500 m, 1,000 m, 1,500 m, and 2,000 m respectively. All other parameters were the same as previous model. The deeper the sand layer, the smaller the signal amplitude on the surface.

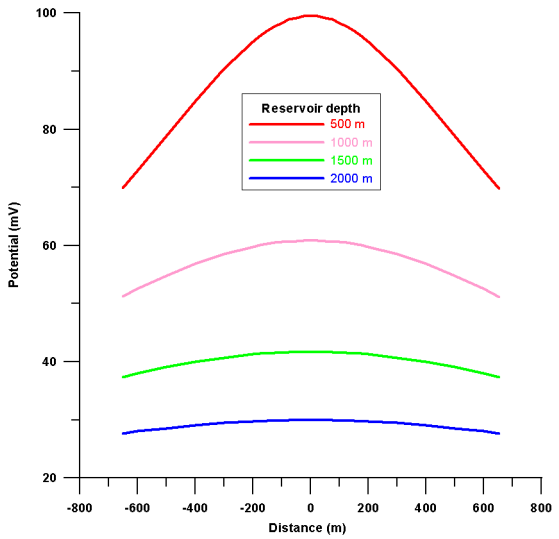

Figure 11. SP response for 100 m thick sand layer at the depth of 500 m, 1,000 m, 1,500 m, and 2,000 m

Another aspect of interest was how the CO_2 flow rate influenced SP response. **Figure 12** illustrates that the higher the flow rate, the bigger the SP response. The model used in this figure simulates a 100 m thick layer at a depth of 1,000 m; all other parameters were the same as previous models. The flow rates used in these models were 440 L/s, 293 L/s, and 40 L/s, respectively.

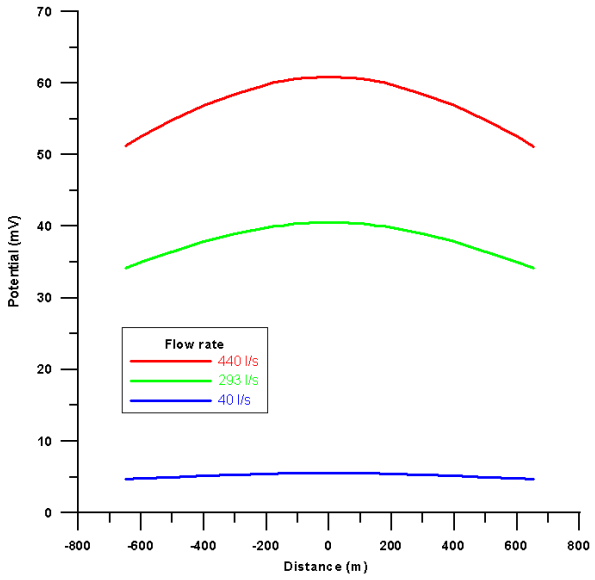

Figure 12. SP response for 100 m thick sand layer at a depth of 1,000 m for the flow rate of 440 L/s, 293 L/s, and 40 L/s

We also studied the relationship between the thickness of the layer and the SP response. To illustrate this concept, we ran a model with 10 m, 30 m, 100 m, and 200 m thick sand layer at the depth of 1,000 m; all other parameters were unchanged. **Figure 13** shows that the amplitude of

the SP response is inversely proportional to the thickness of the layer. The largest response was for the 10 m thick layer. This result derives from the SP response being linearly proportional to the fluid flux, Γ in Equation (1), so that for a given injection rate, the thinner layers have a higher fluid flux Γ.

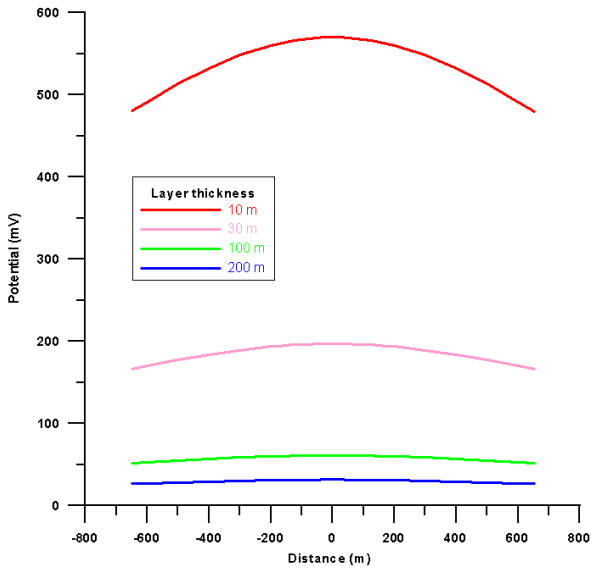

Figure 13. SP response of the 10 m, 30 m, 100 m, and 200 m thick sand layer at the depth of 1,000 m.

We have also investigated how the SP response depends on the coupling coefficient, L**. Figure 14** shows the results for the Liberty Field.

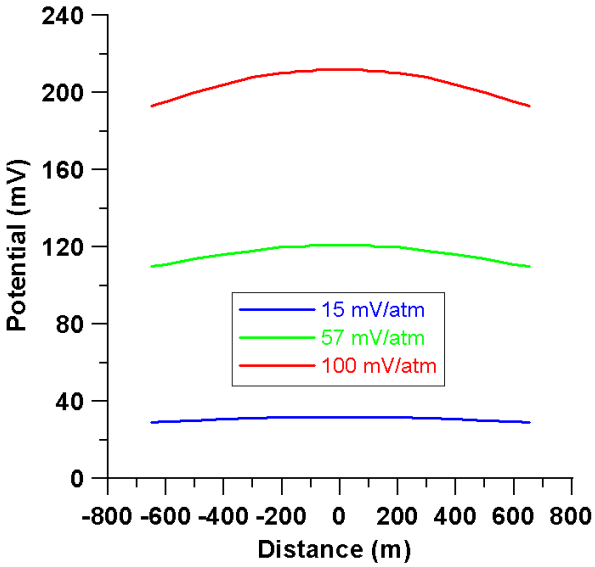

Figure 14. SP response of the Liberty Field reservoir for the coupling coefficient of 15 mV/atm, 57 mV/atm, and 100 mV/atm.

The Liberty Field is a 10 m thick layer at 1,500 m depth, with a lateral extent of 500–600 m. Its permeability is 150 milliDarcies, the flow rate is 4 L/s, and the viscosity of CO_2 is 73 μPa-s. The model was run for three different values: 15 mV/atm, 57mV/atm, and 100 mV/atm, representing a linear progression from potable water (L=15) to resistive benzene (L=100). **Figure 14** shows a linear dependence between the cross-coupling coefficient and the SP response.

Figure 15 shows the SP response caused by the coupling coefficients of 15 mV/atm, 57mV/atm, and 100 mV/atm for the Sleipner field. The Sleipner reservoir has a 100 m thick layer at the depth of 800 m, with permeability 3 darcies, flow rate 44 L/s, and a CO_2 viscosity of 63 μPa-s. Because the Sleipner reservoir is a high-permeability continuous layer, the SP response is much smaller, but probably still measurable for large coupling coefficients.

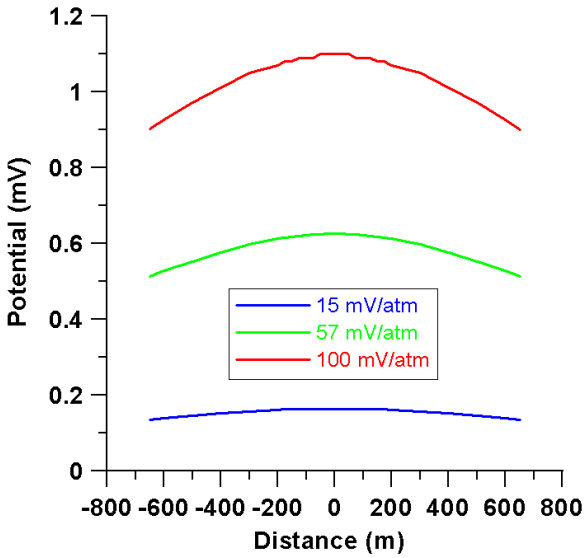

Figure 15. SP response of the Sleipner reservoir for the coupling coefficient of 15 mV/atm, 57 mV/atm, and 100 mV/atm

Gravity Modeling

To set some limits on the size and depths of CO_2 plumes that can be detected and resolved by surface gravity measurements, the wedge model shown in **Figure 16** was used. The top of the wedge is at a depth of 2,000 m, with a variable thickness and radius.

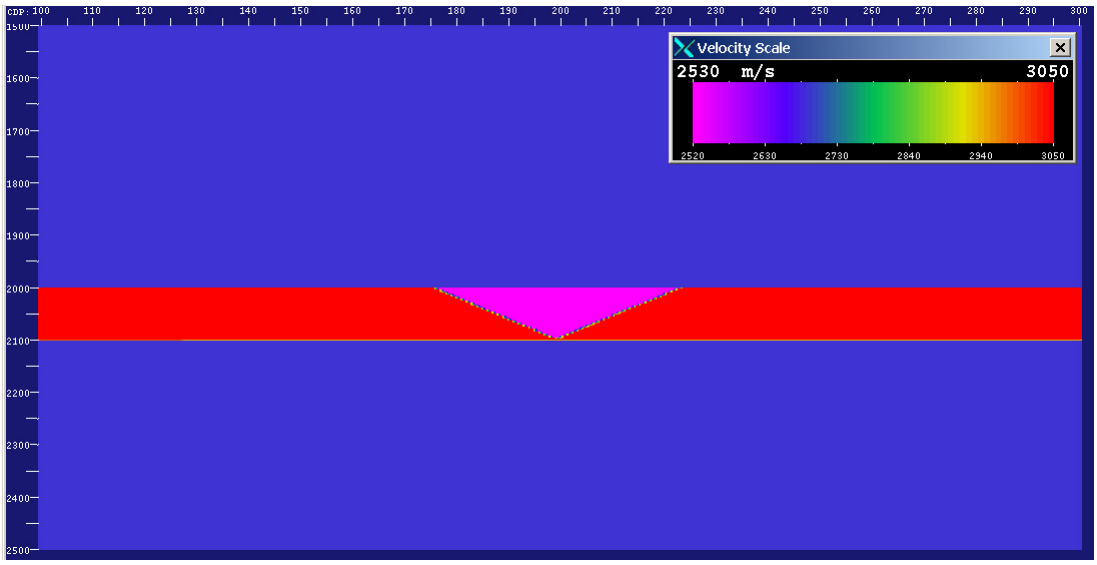

Figure 16. Velocity model of the CO_2 wedge placed in a sand layer (red) surrounded by shale (blue) at a depth of 2,000 m.

The rock parameters were taken as general onshore Texas values of density. The surrounding shale was modeled with a density of 2.24 kg/m^3 and a brine-saturated sand layer (density of 2.28 kg/m^3) having 20% porosity. The 3D wedge of CO_2-saturated sand was considered to be 100% saturated with CO_2, which resulted in a density of 2.20 kg/m^3 for the wedge.

Figure 17 shows three surface response curves for the vertical component of the gravity field at the top of the wedge (2,000 m depth). The radius of the wedge is 240 m. The simulation was run for three w edge thicknesses: 100, 50, and 30 m. A reasonable number for land-gravity-measurement sensitivity levels is 2 micro-gals (μGal). At this depth, even the response of the 100 m thick wedge is below this level. Since the response of the 100 m thick wedge is just below the 2 μGal level, we conclude that volumes corresponding to 41 days of injection could typically be detected but not resolved.

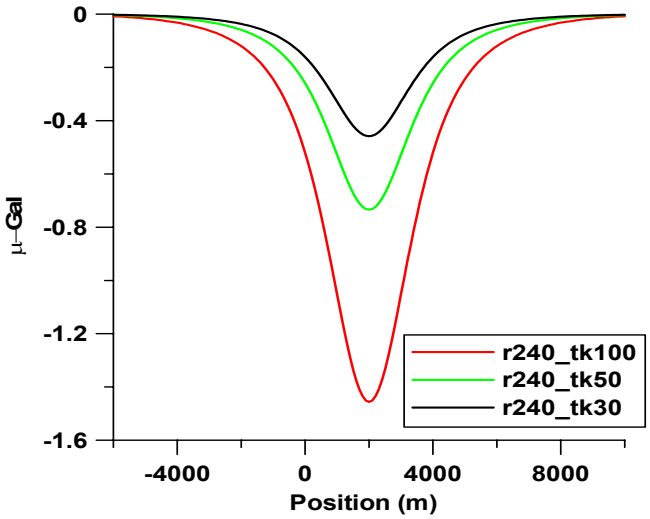

Figure 17. Surface vertical component of gravity measured over a 3D wedge at a depth of 2,000 m. The wedge radius is 240 m, with thicknesses of 100, 50, and 30 m. The wedge with a thickness of 100 m contains the equivalent amount of CO_2 produced by a 1,000 MW coal-fired power plant in 41 days.

A second set of models with the wedge at 1,000 m depth were run; their responses are shown in **Figure 18**. With the CO_2 plume at 1,000 m, both the 50 m and 100 m thick volumes are detectable. The observed gravity response for the 100 m wedge is large enough to be resolved to some degree. Further inversion of the gravity responses will be required to determine what level of model resolution is achievable with these data.

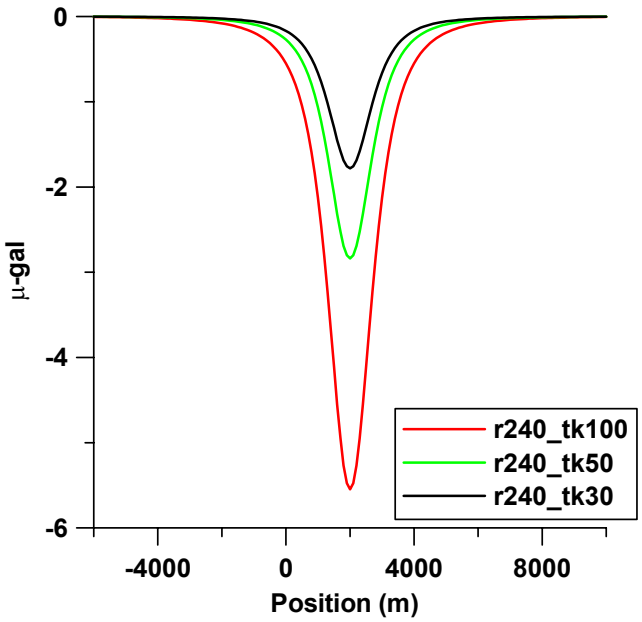

Figure 18. Surface vertical component of gravity measured over a 3D wedge at a depth of 1,000m. The wedge radius is 240 m, with thicknesses of 100, 50, and 30 m.

Our conclusions to date are that, most likely, gravity will be the only useful monitoring method for accumulations of CO_2 at depths less than or equal to 1 km. The volumes affected for deeper targets will have to be much larger. These results are model specific to the Texas Gulf Coast. Further work will compile a list of expected density contrasts between sand and shale in other prospective CO_2 sequestration areas, with a full range of CO_2 accumulation sizes at a range of depths. We expect that this more comprehensive analysis of gravity responses will be completed in the third quarter (coming quarter) of the project.

Surface electromagnetic mapping

We have acquired a new version of a 3-D modeling and inversion code written by Greg Newman from Sandia National Laboratory, which we plan to use for our surface electromagnetic mapping. In addition, we obtained a full set of data (e.g., well logs, seismic, reservoir properties, results of flow modeling studies) on the Schrader Bluff field, on the Alaskan North Slope. We will use these data as well as those of the Liberty field to test the applicability of EM methods to monitor CO_2 injection.

Figure 19 is a model that we used to test the code against previously published results. The model consists of a 100 x 400 x 50 m, 3 Ohm-m block at a depth of 50 m in a 100 Ohm-m background. A vertical magnetic dipole was used as a source.

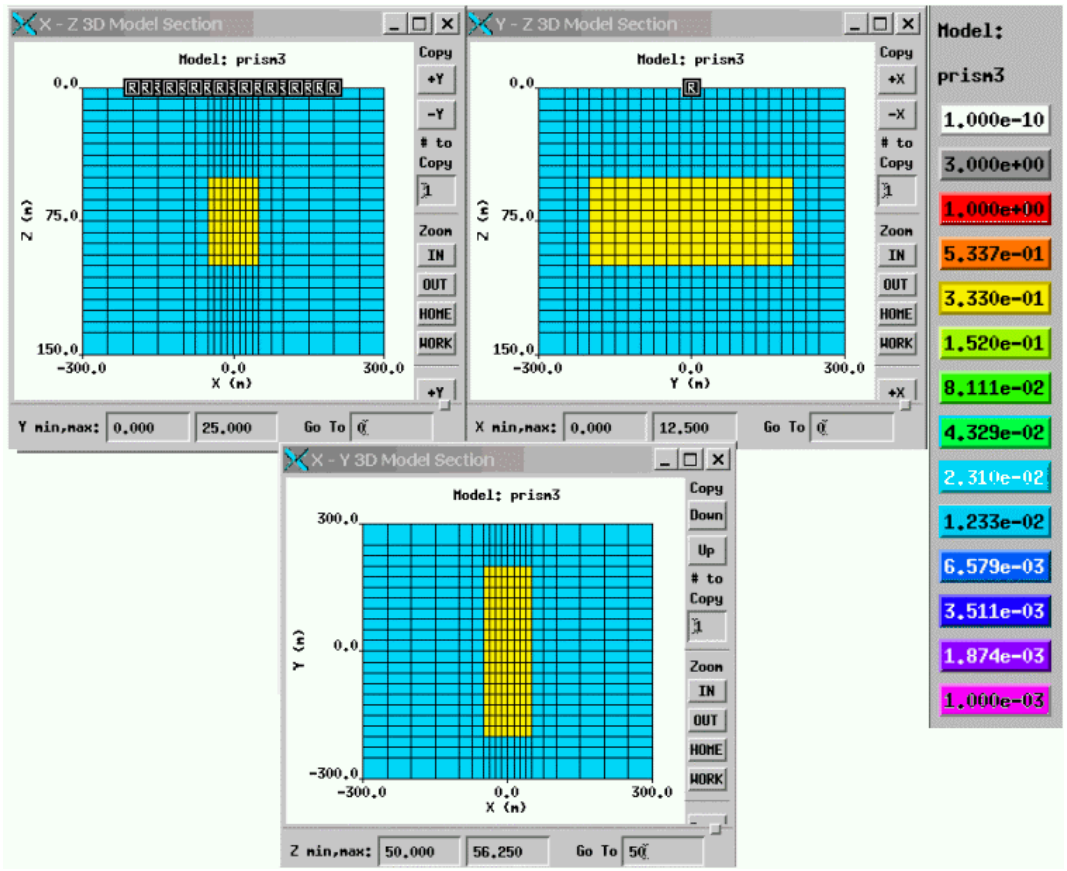

Figure 19. 100 m x 400 m x 50 m block of 3 Ohm-m at a depth of 50 m in a 100 Ohm-m background.

The real (in-phase) and quadrature components for this model are shown in **Figure 20**. The results from the new code show good agreement with previous ones. The code is now ready for simulation of magnetic and electric dipole sources in a surface measurement mode over the Schrader Bluff sequestration time-lapse models.

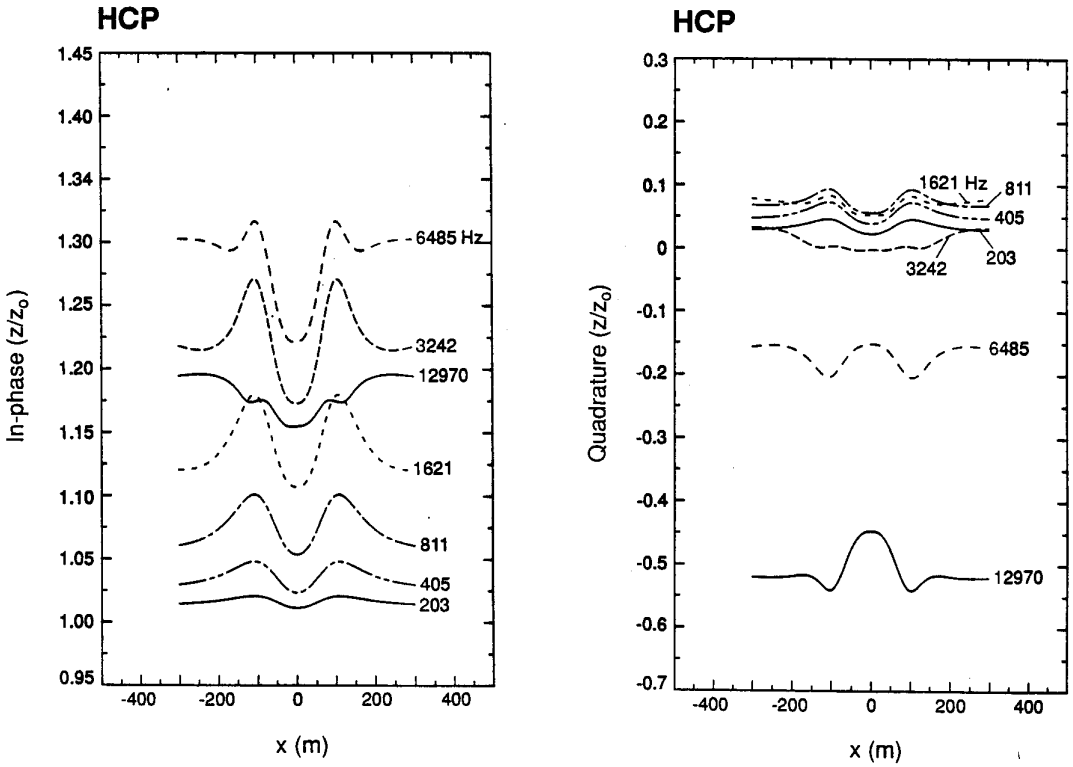

Figure 20. Real (in-phase) and quadrature components for the model from **Figure 18**

Work Next Quarter

Laboratory measurements of SP coupling coefficient for CO_2 injection into Frio sands (in support of Task E) need to be finalized.

Surface SP measurements need to be made during the upcoming Frio tests, and models need to be used to infer spatial distribution of CO_2 from the SP data (in support of Task E).

VSP and crosswell seismic Frio information needs to be processed, interpreted, and then integrated with the SP data (in support of Task E).

Subtask B-2: Field Data Acquisition for CO_2 Monitoring Using Geophysical Methods

Goals

To demonstrate (through field testing) the applicability of single-well, crosswell and surface-to-borehole seismic, crosswell electromagnetic (EM), and electrical-resistance tomography (ERT) methods for subsurface imaging of CO_2.

Previous Main Achievements

- The first test of the joint application of crosswell seismic and crosswell electromagnetic measurements for monitoring injected CO_2 was completed.

Accomplishments This Quarter

- We refined a scoping study of tiltmeter methods to detect and monitor CO_2 injection as part of the Frio Brine Pilot Project (Task E). Simple dislocation modeling, based on calculated

pressure changes resulting from the injection of 5,000 tonnes of CO_2 indicate that tilt generated by deformation of the Frio B sand reservoir would be detectable by surface tiltmeters

- We conducted a time-lapse electrical-resistance tomography (ERT) casing survey in the Vacuum Field, New Mexico, where CO_2 injection is underway.

Progress This Quarter

Work focused on evaluating the potential for tiltmeter surveys to assess CO_2 injection during the Frio Brine Pilot (Task E) and in conducting time-lapse ERT casing surveys at the Vacuum Field.

Electrical-Resistance Tomography (ERT)

During normal field operations in September, a time-lapse casing survey was obtained over the 11-well pattern in the Vacuum Field. The data were processed and the results are being analyzed in conjunction with production records from the field. The survey was collected with all wells under normal operations (pumping and injection). Field measurements remain consistent, with acceptable data quality obtained during those operational conditions. The September survey displays higher resistivity in the northern region, which is consistent with the area in which CO_2 is being injected. However, during this period, CO_2 injection rates have been low because of production issues. Thus, any change due to CO_2 is not expected to be substantial over this time frame.

The time-lapse data correlate with other aspects of the production history. The primary change over the four-month period is a decrease in electrical resistivity of a few percent over a portion of the field. This decrease is most significant in the vicinity of the well in which a pronounced increase in oil/water ratio had been obtained in response to water injection. The overall area of decreased resistivity is coincident with the region of greatest fluid injection and movement. These results can be interpreted in terms of water displacing oil in the pore spaces, which is consistent with both the injection and production results. The second-most pronounced change in field resistivity occurs in the vicinity of the well that experienced the second-highest increase in oil/water ratio over the same time period.

A subsequent time-lapse casing survey is scheduled for early December. This survey will extend the well pattern to an area where CO_2 injection is just starting. The larger pattern will incorporate two different CO_2 injection scenarios—one during startup, the other during longer-term injection. Key issues to address include the measurement design to optimize rapid data collection over large patterns.

Tiltmeters

We carried out synthetic modeling of the ground surface deformation possibly resulting from injection of 5,000 tonnes into the brine-saturated Frio B sand at the South Liberty field (Task E). This effort enables a preliminary assessment regarding the feasibility of using surface tilt measurements to map the subsurface distribution of CO_2 volume and pressure as a function of time through the pilot test. This assessment is based on (1) whether the surface deformation is large enough to be detected by high-sensitivity tiltmeters, and (2) whether the deformation pattern is diagnostic of the spatial distribution of CO_2 within the formation.

Modeling: The deformation modeling we have carried out to date is preliminary and intended to provide order-of-magnitude estimates of surface tilt amplitudes and patterns. Pore pressure distributions calculated from preliminary flow modeling performed by LBNL (using TOUGH2) provided the basis for the deformation modeling. This modeling is described at http://esd.lbl.gov/GEOSEQ/pilot_sims/pilot_sims_main.html . Specifically, we used the pressure distributions resulting from the base homogeneous model UQ02 at 100 days, provided by Chris Doughty, LBNL.

We represented the entire 6 m thick upper B sand layer as a single thin square slit inflated by the increase in pressure, ΔP, above initial hydrostatic conditions. The inflated slit was modeled as a finite opening-mode dislocation (**Figure 21**) having x (SE, along strike) and y (NE) dimensions of 170 m, based on the zone of significant gas saturation and pressure increase in the flow model. The dislocation dips 15° SW and is centered within a homogeneous elastic half-space at a depth of 1500 m. This source model is appropriate given the large (≈30) ratio of length to thickness of the flow zone. The pressure increase throughout the slit was assumed to be a uniform 0.6 Mpa, taken as the average of the ΔP profiles along *x* and *y* through the injection well shown in **Figure 22.** The normal opening (Burger's vector), u_z, of the dislocation was estimated using the relation (Sneddon, 1946) between the normal displacement, $u_z^{\max}$, at the center of a uniformly pressurized circular ("penny-shaped") crack equal in area to the square dislocation:

$$u_z^{\max} = \frac{2(1-\upsilon)}{\pi\mu} a\Delta P$$

where ν, μ and a are Poisson's ratio, rigidity, and crack radius, respectively. The uniform opening (u_z) of the dislocation was taken as the average of the elliptically shaped distribution of displacement of the Sneddon crack. The circular crack and square dislocation models generate almost identical surface deformation fields when the source depth is greater than about twice the source dimension (e.g., Davis, 1983). Surface tilt fields were computed with the computer program SYNEF (B. Foxall, unpublished), which utilizes the dislocation Green's functions of Okada (1985).

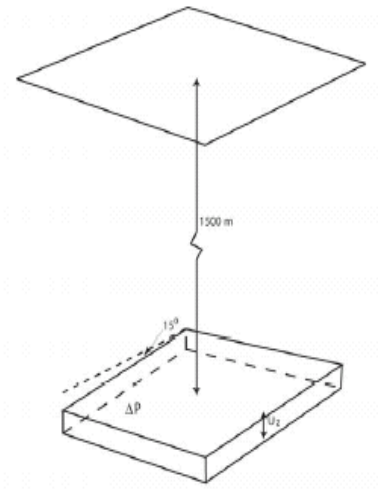

Figure 21. Dislocation model

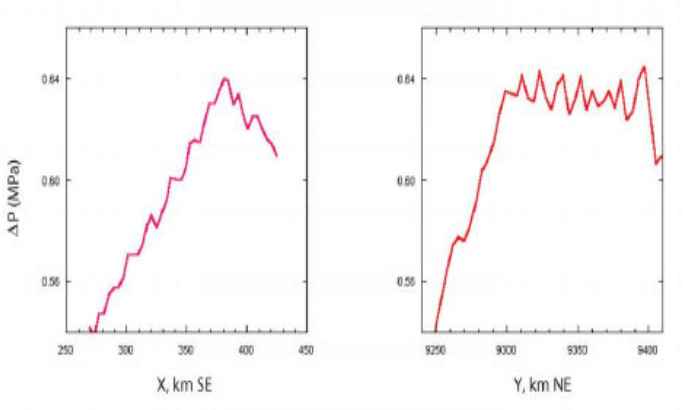

Figure 22. Pressure change profiles along X and Y through the injection well (from LBNL TOUGH2 model UQ02). X and Y coordinates correspond to the LBNL model.

Choice of the half-space elastic constants influence the calculated surface deformation, not only through the Green's functions but also in the estimation of u_z by the above relationship (and hence the source strength). We have not yet investigated the elastic properties of the specific formations at the South Liberty field, so for these preliminary simulations, we used two generic sets of values for sedimentary rocks. The elastic constants and resulting source dislocation displacements are given in **Table 1.**

Table 1. Half-space elastic constants and opening displacements resulting from uniform pressure increase of 0.6 MPa

Model	ν	μ (MPa)	u_z (mm)
1	0.30	1.0×10^4	4.0
2	0.25	1.5×10^4	2.9

Discussion of Results: The surface tilt fields computed from the two models are shown in **Figure 23**. Model 1 predicts tilt values in the range 10–20 nanoradians, which should be detectable with an array of tiltmeters installed in shallow (6–12 m) boreholes. Modern tiltmeters routinely deployed for hydrofracture monitoring and mapping are generally capable of detecting signals as small as 10 nanoradians or less under typical oilfield noise conditions. Model 2 also predicts detectable surface tilt, but tilt amplitudes are lower and approach the detection threshold.

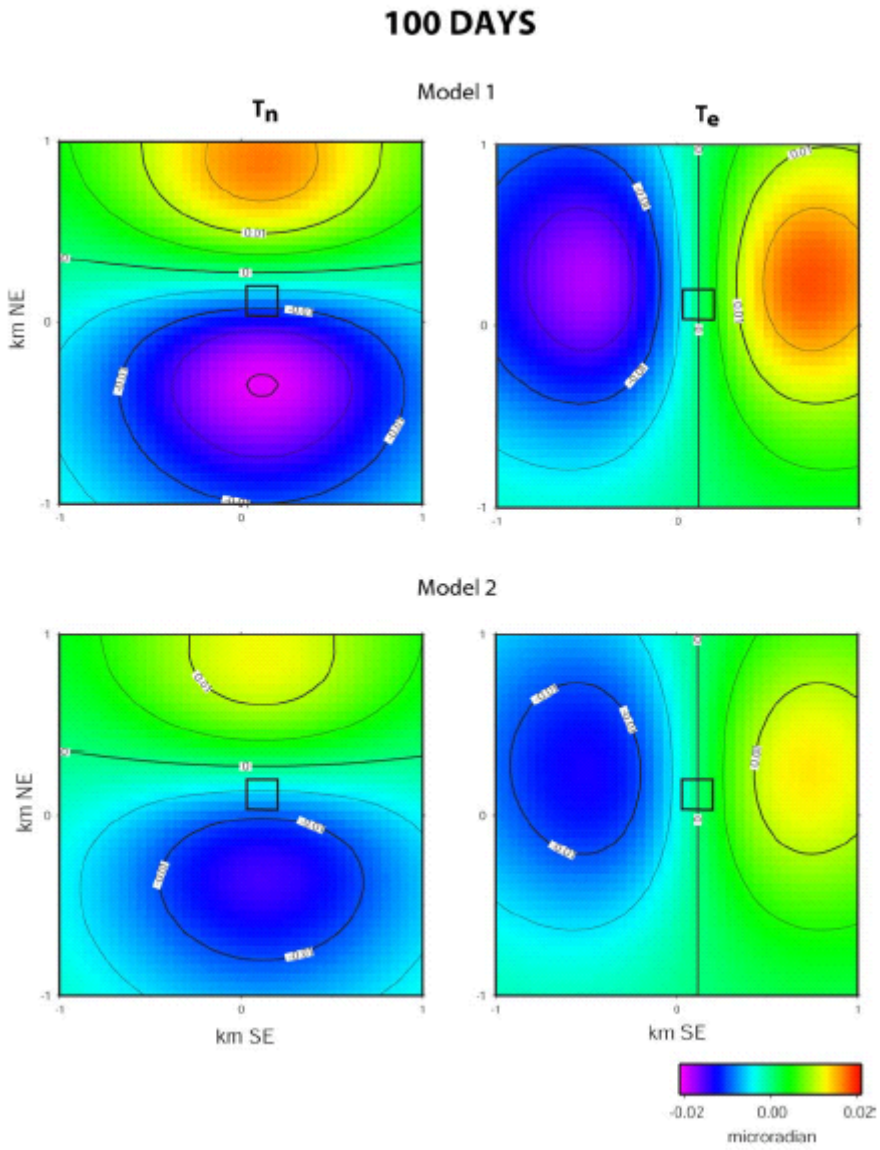

Figure 23. North and south components of surface tilt for Models 1 and 2. Contour interval is 0.005 microradians. Dislocation source is shown as black square.

Figure 23 shows that the surface tilt field is sensitive to the change in fluid volume within the source layer. However, tilt probably would not provide constraint on the shape of the pressurized, gas-infiltrated zone because of the large (≈9) ratio of source depth to source dimension. This is indicated by the close similarity of the Model 1 finite source tilt field in **Figure 23** to that generated by a *point* source of equal strength shown in **Figure 24.** Significant asymmetry in the CO_2 and pressure distribution that results in a shift of the source centroid would likely be detectable. However, with the possible exception of the UQ07 model (combined injection and pumping, low pressure), such asymmetry is not seen in the LBNL models.

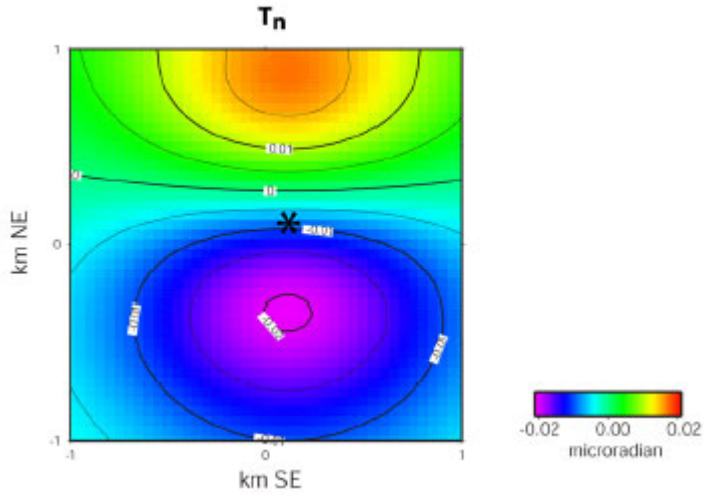

Figure 24. North components of surface tilt from a point source equivalent to Model 1. Source location shown by star.

Conclusions: Simple dislocation modeling, based on pressure changes simulated by TOUGH2 modeling of the injection of 5,000 tonnes of CO_2, indicate that tilt generated by deformation of the Frio B sand reservoir would be detectable by surface tiltmeters. While the modeling indicates that tilt field would be sensitive to the volume and pressure changes within the reservoir, it also suggests that the tilt field may not be diagnostic of the shape of the CO_2 plume, owing to the depth of the reservoir relative to the calculated dimensions of the plume. The modeling results are somewhat sensitive to the choice of elastic properties, and more refined modeling should use the actual elastic parameters that may be available for formations within the South Liberty field. The highly idealized modeling discussed here treats the entire CO_2-filled layer as a single dislocation source and (like the TOUGH2 modeling) does not consider the actual poroelastic mechanism of deformation within the reservoir. In effect, the models assume that all of the change in fluid volume in the reservoir is converted to strain in the surrounding medium.

References

Davis, P.M., Surface deformation associated with a dipping hydrofracture. Jour. Geophys. Res., 88, 5826–5834, 1983.

Okada, Y., Surface deformation due to shear and tensile faults in a half space, Bull. Seismol. Soc. Am., 75, 1135–1154, 1985.

Sneddon, I.N., The distribution of stress in the neighborhood of a crack in an elastic solid, Proc. Roy. Soc. (London), 187, 229–260, 1946.

Work Next Quarter

- The use of tiltmeters during the Frio Brine Pilot Project will be assessed with respect to the actual project plans and more specific field model(s).

- A time-lapse ERT survey will be obtained in the Vacuum Field in December over a much larger region, which will provide a baseline for a portion of the field in which CO_2 injection is starting. Field data will be processed and interpreted.

Subtask B-3: Application of Natural and Introduced Tracers for Optimizing Value-Added Sequestration Technologies

Goals

To provide methods that utilize the power of natural and introduced tracers to decipher the fate and transport of CO_2 injected into the subsurface. The resulting data will be used to calibrate and validate predictive models utilized for (1) estimating CO_2 residence time, reservoir storage capacity, and storage mechanisms; (2) testing injection scenarios for process optimization; and (3) assessing the potential leakage of CO_2 from the reservoir.

Previous Main Achievements

- Laboratory isotopic-partitioning experiments and mass-balance isotopic-reaction calculations have been done to assess carbon- and oxygen-isotope changes (focused on the influence of sorption) as CO_2 reacts with potential reservoir phases.

Accomplishments This Quarter

- Gas and isotope compositions have been determined for wells sampled on 6/12/02 at Lost Hills, California, which indicate a substantial contribution of injection CO_2 in select wells compared to the previous sampling on 2/14/02.

- Pressure, flow, and helium porosimetry testing on the dynamic flow system are near completion.

- Detailed experiments have been conducted on perfluorocarbon tracer gas-chromatography analytical methods, reproducibility, and sensitivity as a prelude to tracer flow experiments.

Progress This Quarter

Gas Chemistry and Stable Isotopes

Gas compositions (CO_2, C_1-C_6, N_2, O_2) have been measured for samples obtained from Lost Hills, California, on June 20, 2002, toward the end of a modest CO_2-injection period that started in early May. Isotope compositions were also measured on the CO_2 injectate, as well as CO_2 and CH_4 separated from the production gases. The gas chemistries are plotted together with results we had obtained previously from earlier samplings on CO_2-CH_4-ΣC_2-C_6 ternaries shown in **Figure 25**. Clearly, the contribution by injectate CO_2 has become more pronounced with an increase in time since the Feb. 14 sampling for some wells (11-9J, 11-7B, 12-7), but only slightly so for other wells (12-8D and 11-8D). In fact, gas chemistry for Well 11-8D is very close to the gas compositions determined for wells sampled prior to the initiation of the CO_2 injection test (9/19/00), which we assume represents the “baseline” reservoir chemistry. Interestingly, gas chemistry from Well 11-7B plots even closer to the methane corner of the ternary, suggesting that the baseline for this well may be even more methane-rich than previously assumed, based on our sampling of wells prior to the CO_2 injection test. This well was not one we sampled prior to initiation of the DOE injection test. As we have pointed out in previous reports, the gas and isotope chemistry of true reservoir

gas will never be known for this area because of the long history of perturbation—i.e., water injection.

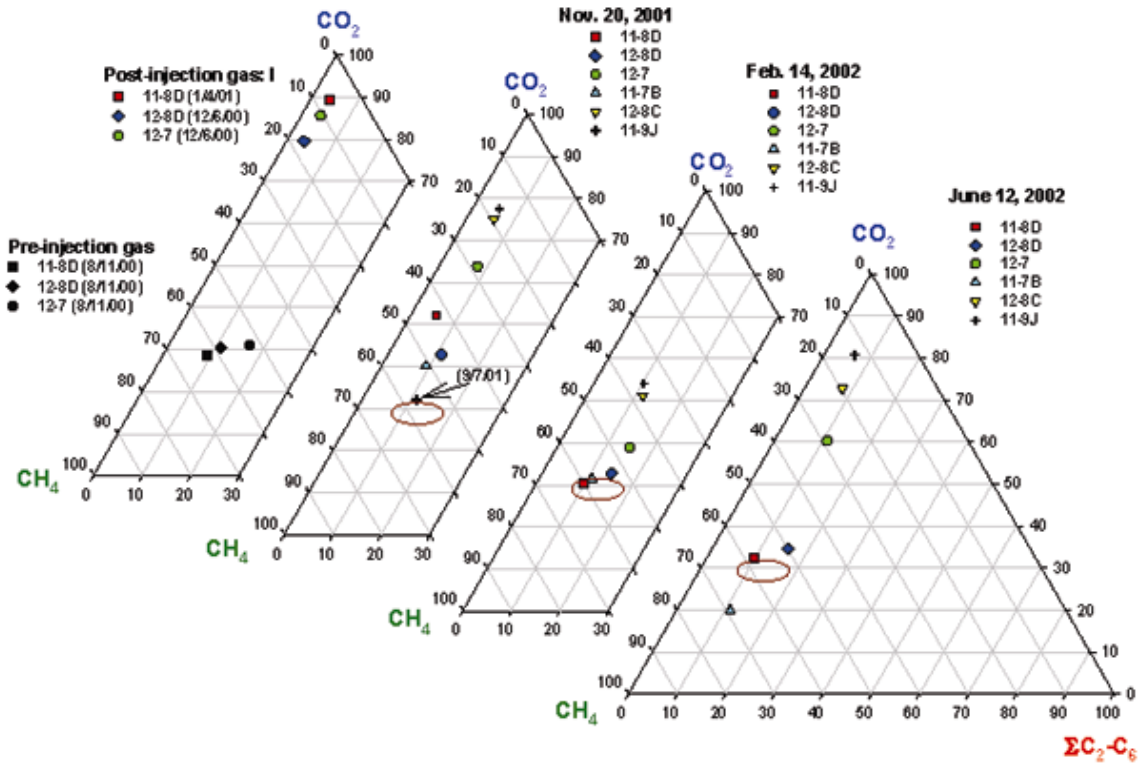

Figure 25. Gas compositions of samples obtained from the Lost Hills, California, injection system

With this most recent sampling, we now are getting a better sense of the shifts in gas chemistry and isotopes over a time frame of a few months by comparing chemistries from Well 11-9J sampled on 9/7/01, 11/20/01, 2/14/02, and 6/12/02. The first and third of these sample times occurred at the end of water injection episodes, whereas the second and fourth sample dates fall just a few days after CO_2 injection was stopped, and during it, respectively. The gas chemistry is clearly more "reservoir"-like during water injections, particularly for the 9/7/01 sample, which was associated with a longer-duration, higher-capacity injection compared to 2/14/02. Note that in **Figure 25** the 2/14 sample has a gas chemistry intermediate to the 9/7/01 and 11/20/01 samples, and that the CO_2 content from the June sampling is the highest recorded for this well during our study. Results from additional samples obtained in October of this year will help us confirm the cyclic nature of the CO_2 content as a function of time and alternation of CO_2 and water injections.

The carbon isotope compositions of CO_2 are plotted as a function of time in **Figure 26**. For some wells, it appears that isotopic values determined for samples obtained during intervals of CO_2 injection are more depleted in ^{13}C compared to samples obtained during or just after water injection. This is consistent with an increased contribution of injectate CO_2, which has a very negative carbon isotope signal (~ -30 per mil) compared to the "reservoir" CO_2. For example, in our last sampling on June 12, we observe substantially more negative $\delta^{13}C$ values for Wells 11-9J and 12-7 compared to the Feb. 14 sampling, but a somewhat modest shift to a more depleted value for Well 12-8C. In fact, the carbon isotope compositions of these three wells mimic those observed from the Nov. 20, 2001, sampling, which also was conducted during a period of CO_2 injection. At no time, however, have the gas chemistries ever exhibited as rich a CO_2 content, nor as negative a carbon isotope value, as were observed in the very first samples obtained at the end of the first (and most intense) CO_2 injection period (9/00 –12/00). Because Wells 12-7 and 11-9J/12-8C are located at opposite corners of the four 2.5-acre well pattern, separated by major

faults, the increase in CO_2 concentration (along with more negative carbon isotopes) is clearly a consequence of communication with the closest injector wells, 12-7W and 11-8WA, respectively. Tracking the changes in chemistry and stable isotopes is complicated by the fact that the durations and capacities of separate injections of water and CO_2 have varied over time, as was which set of wells was used during a particular injection test. Once we have obtained our final set of analyses from the October sampling (in progress), we will begin to sort out the impact of these complexities.

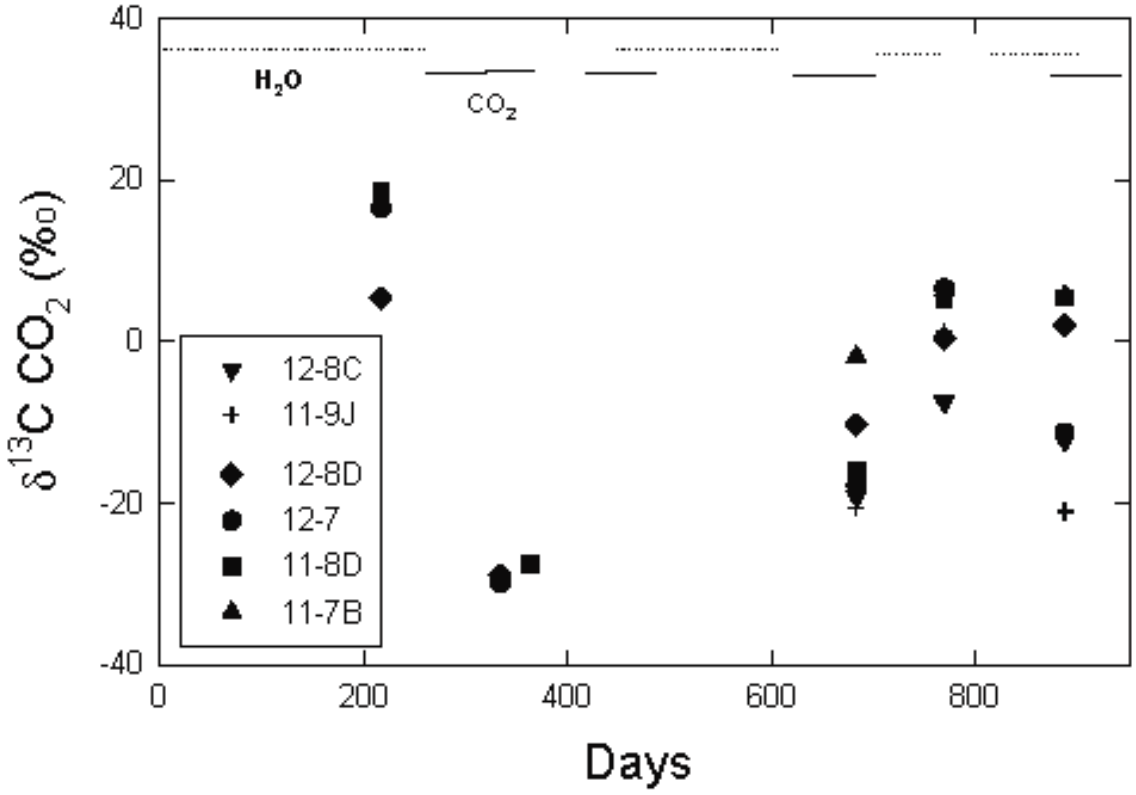

Figure 26. Plot of CO_2 carbon isotope values (in per mil) determined for "reservoir" samples (taken August 18, 2000, prior to CO_2 injection; 224 days after initial water injection), and CO_2 separated from samples obtained from various wells in the Lost Hills, California, system over time. Also shown are the intervals when either water or CO_2 was being injected (top of figure).

Applied Gas Tracer Studies

Flow System Testing: We near the final pressure- and flow-testing stage of the dynamic flow system shown in **Figure 27**. Helium, nitrogen, and pure water were used in these tests. This system gives us the capability of assessing the relative interactions of gas tracers, such as SF_6, and an assortment of perfluorocarbons (PFCs) with a variety of reservoir materials, over a range of temperatures (up to ~80°C) and pressures (up to 300 bars) appropriate for proposed injection scenarios. The system is comprised of several features: (a) carrier gas and He reservoirs, (b) brine reservoir, (c) tracer gas injection volume, (d) gas homogenization reservoirs, (e) brine flow line, (f) sample loop, and (g) gas chromatograph. Helium is used to sparge other gases as well as in measuring the porosity of the solid contained in the sample loop. The sample coil is 20 feet long (or 40 feet if need be) and has been initially filled with Ottawa sand (0.5–0.8 mm diameter grain size). The sample coil length and diameter can be varied according to the specific application. Brine or hydrocarbon can be pumped into the coil prior to initiating gas flow. The brine line and the

coil are composed of 2507 steel, which is highly resistant to corrosion. Carrier gas and tracer gas(es) are thoroughly mixed prior to flow in gas homogenization reservoirs. Multiple flow paths permit repeated “reloading” of the system with carrier gases that contain different types and amounts of tracer gases. Pressure and flow are generated by use of either a HPLC pump or manual screw-press. Pressure and temperature are monitored and recorded continuously during each experiment via a customized version of LabView.

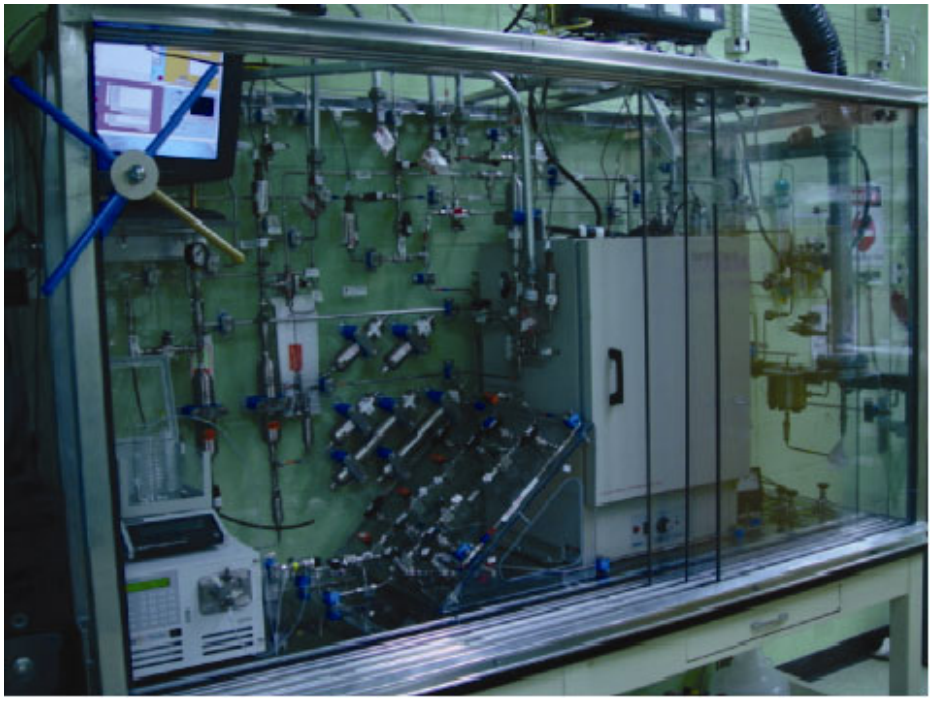

Figure 27. Dynamic flow system built at ORNL. This system is capable of flowing tracer gases with CO_2, brine, or hydrocarbon present across a coiled 20 ft or 40 ft column (not shown, in side furnace) at temperatures up to 80^{o}C and pressures to about 300 bars. The gas chromatograph is off-camera to the right. Also notice a series of Lexan doors on the right used for protective shielding. These can be positioned anywhere along the front of the apparatus by use of the slide tracks. The flow direction is from left to right. An HPLC pump and a manual screw press can be used to generate both pressure and flow.

PFT Chromatography Experiments

Gas chromatography experiments were conducted using nominal 1% solutions of perfluoromethylcyclopentane (PMCP), perfluoromethylcyclohexane (PMCH), and perfluorotrimethylcyclohexane (PTCH). SF_6 was later added to this suite of tracers once a method to separate the 3 PFTs was developed to determine if it, too, could be simultaneously separated using the same method. These experiments had three primary goals: (1) to establish a GC method using a capillary column that could effectively separate the three PFTs and SF_6; (2) to test the stability and consistency of the measurements; and (3) to estimate the sensitivity of the detection method.

Analytical Method: The analytical method uses an HP 5890 GC equipped with an ECD detector because of the high susceptibility of fluorinated compounds to electron capture. N_2 is used as the carrier gas. Initial tests for determining sensitivity and retention times for the PFTs were conducted using HP1 and HP5 fused silica columns and an $AlOH_2$ column that had the following dimensions:

HP1	Column length—60m	Internal diameter—0.25mm

HP5	Column length—50m	Internal diameter—0.53mm
$AlOH_2$	Column length—50m	Internal diameter—0.53mm

Single and multitracer standards were prepared by injecting a known volume of a 1% solution of PFT into a nitrogen-flushed 40 ml EPA vial. The vials were then placed in a water bath and heated to 70 ºC to volatilize the PFTs. It was assumed that at that temperature all of the PFT would move into the headspace. Headspace samples were then drawn (1–10 µl) using a gas-tight syringe that had also been heated to 70ºC to prevent crossover contamination from one sample to the next. Multiple injections of each standard were made at each injection volume to test the reproducibility of the measurements and to trace any sources of error.

Initial column flow rates were determined from the linear velocity of N_2 makeup gas. Split vent flow rates, column flow rates, makeup gas flow rates, and isothermal temperatures were varied to assess which protocols work best of the capillary columns. Sample retention times, peak area, width, and height were recorded for all separate PFTs. The HP1 performed the best in isothermal runs for single tracers in terms of getting the best peak resolution and reproducibility. However, the isothermal method did not effectively separate the peaks in a multitracer mix.

Temperature ramping programs were then tested, based on the boiling points of PFTs, where PMCP boils at 48ºC, PMCH at 76ºC, and PTCH at 125ºC. The initial temperature was set to 50ºC and raised 50ºC every 40 seconds until a final temperature of 150º C was reached. A variety of temperature programs and flow rates were tested, but peak separation was never effectively achieved with the HP1 column. Thus, an $AlOH_2$ column was chosen for the next round of trials. Good separation of the 3 PFTs tested was achieved using this type of column. In addition to individual peaks for PMCP and PMCH, four isomers of PTCH were detected using this method. The method did not achieve complete baseline separation of the PTCH isomers. However, this was deemed not to be a problem for this application, since the peak height and area calculations are consistent and the isomers will not be used as separate tracers. The final method chosen uses a detector temperature of 120–150ºC.

Figure 28 shows the retention curve for the suite of 3 PFTs. SF_6, discussed later, is also shown on this curve. The final suite of tracers will include perfluoro-dimethylcyclohexane (PDCH) as well, which will have an elution time somewhere between PMCH and PTCH, based on its structure and molecular weight. Perfluoro-dimethylcyclobutane (PDCB) was also considered for these experiments, but was discarded as a first choice because the elution time is likely to be very similar to that of PMCP. The molecular weight and formula of PMCP and PDCB are identical and, therefore, the diffusive and partitioning behaviors (dependent on molecular weight and number of carbons, respectively) are likely to be very similar as well.

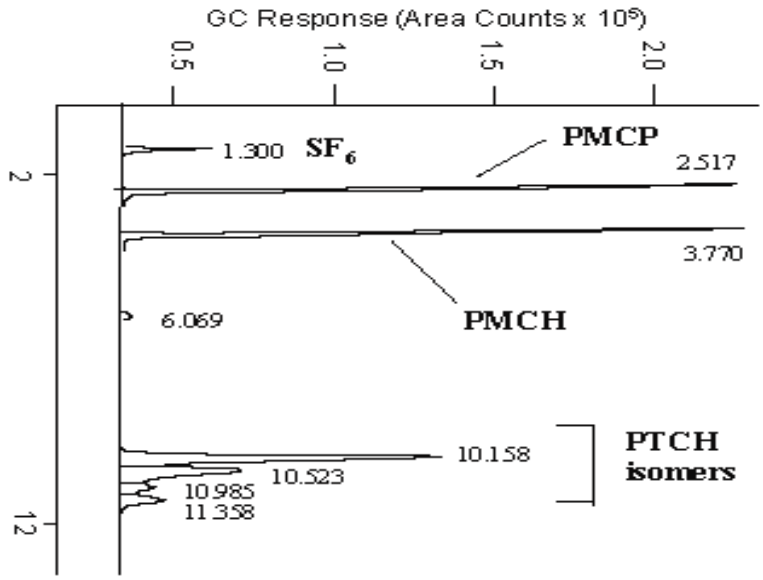

Figure 28. Tracer retention curves using an $AlOH_2$ column and temperature ramping program

Reproducibility and Experimental Error: Numerous analyses were made from single and multi-tracer standards made from the 1% solutions as described above. Replicate analyses showed an inconsistency in reproducibility for a given headspace sample. Potential sources of error include contamination from previous samples, background contamination in the laboratory, insufficient time for volatilization of the PFTs into the headspace, loss of tracer through the EPA vial septum over time, and small variations in the volume withdrawn from the headspace sample. Because of the high sensitivity of the analytical method, even small differences in tracer mass can produce a large difference in the analytical result.

The ratio of the tracer concentrations (expressed as area counts based on a linear response) for a suite of tracers (and for the isomers, in the case of PTCH) was evaluated and found to be very consistent, even with 20% or greater standard error among replicate samples. This suggested that the sources of error were affecting all of the tracers equally, a fact that is reassuring since it is the ratio of the tracers in tracer separation experiments that is of greatest interest. **Figure 29** shows a plot of the ratio of PMCP and PMCH for headspace samples taken from two different multitracer standard solutions. Data will show a linear relationship where the concentration ratios are consistent, as is seen in the plot.

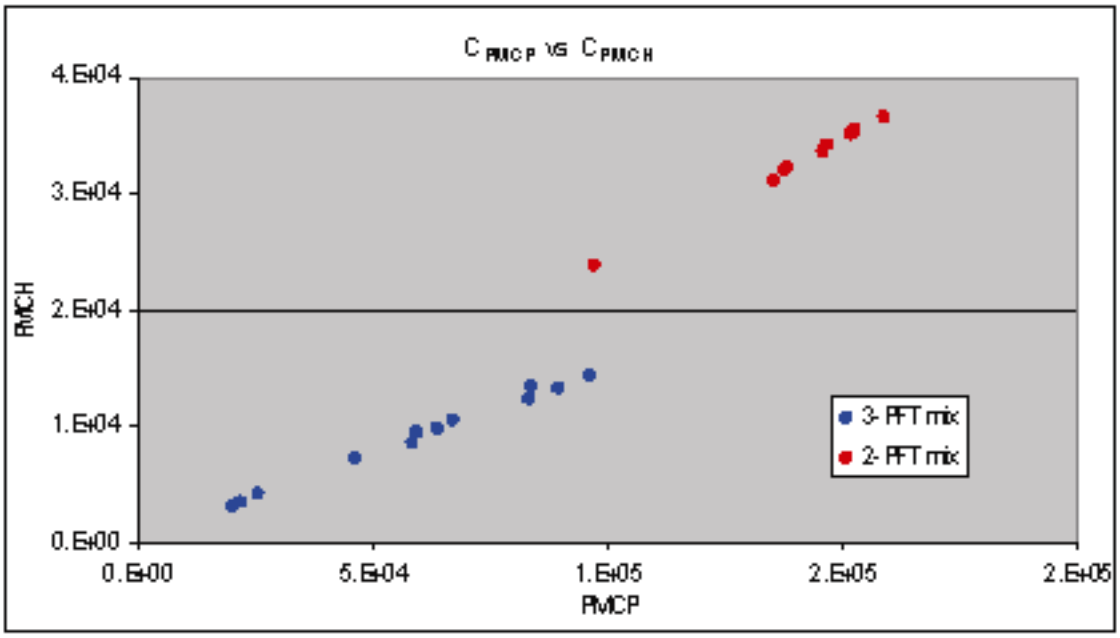

Figure 29. PMCP versus PMCH area counts for two multitracer standards, showing consistency in the concentration ratios (linear behavior)

Examination of the data revealed a pattern of increased GC response for successive injections in many cases, which suggested that the standards had not been given sufficient time to reach equilibrium in the headspace while sitting in the water bath. A test of successive PTCH injections demonstrated this effect (**Figure 30**). The initial series (Series A) was not sufficiently long, and a second series of injections (Series B) indicated that a 90-minute minimum equilibration time is required before headspace samples are obtained for analysis. Because this observation was made after most of the analyses had been completed, and no record was made of how long the standards were heated prior to analysis, it isn't possible to determine how much of the variability in the previous analytical results can be attributed to this source of error. However, it is likely to be a significant contributor, perhaps creating the majority of the variation. That would explain the inconsistency in repeatability from one series of injections to the next, where some sets showed very little variation between successive samples. In **Figure 31**, ratios of the PTCH isomer concentrations are plotted for the same samples shown in **Figure 30**, and it can be seen that the ratios stabilize very quickly, even before actual concentrations come to equilibrium. Based on these observations, sample preparation procedures have been adjusted to insure equilibration in the headspace before analysis.

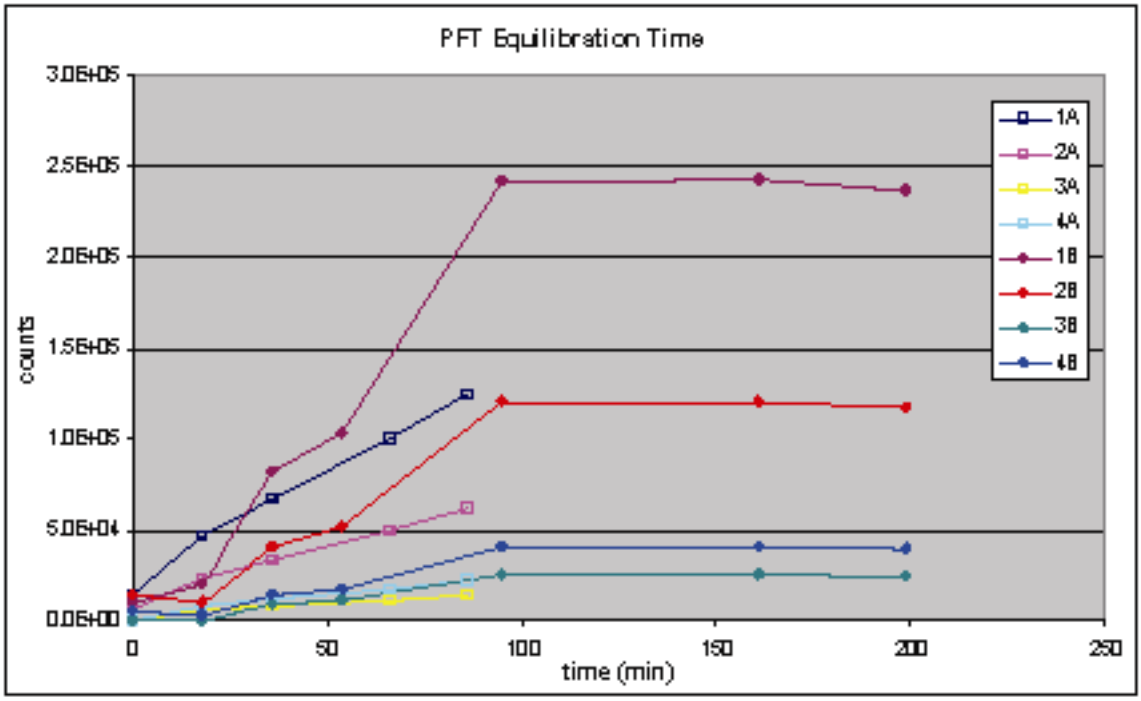

Figure 30. PFT concentrations versus time for successive headspace samples from two PCTH standards (A and B). The numbers represent different isomers of PTCH.

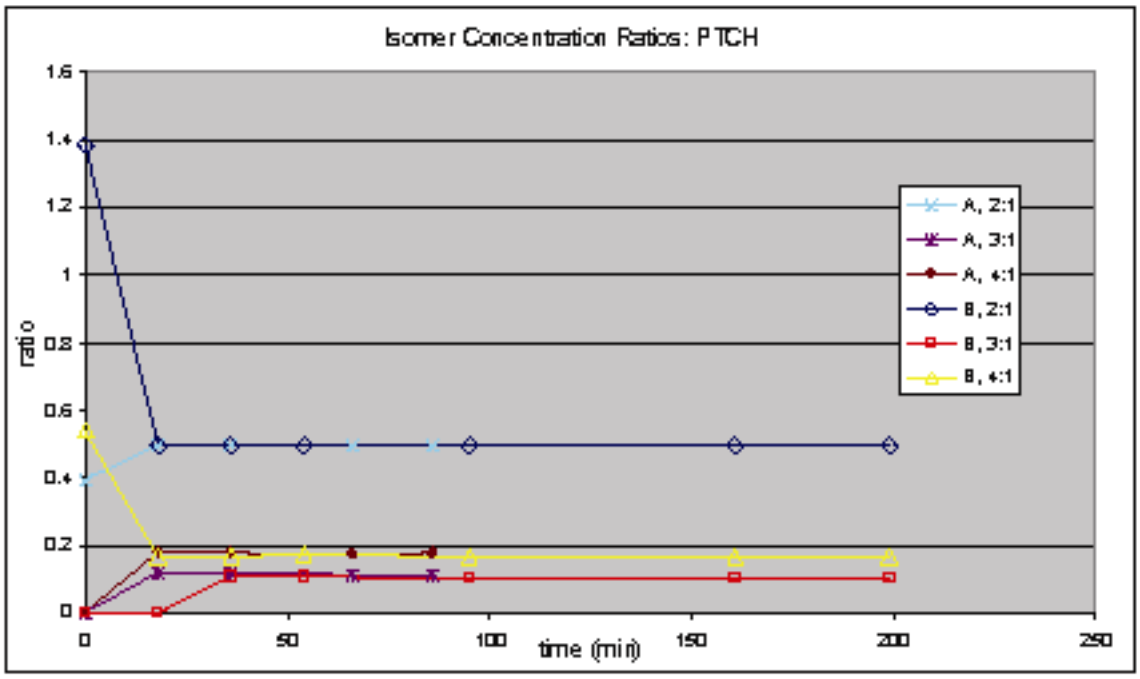

Figure 31. PTCH isomer concentration ratios for the same samples shown in **Figure 29**

In a final round of injections, SF_6 was added to one of the 3-PFT standard mixtures to determine if the peak could be separated from the PFTs using the same GC method. Data for these experiments are included in the Appendices and demonstrate that SF_6 could be resolved. The

peak is seen in the GC output shown in **Figure 28**. One difficulty that arose, however, is the presence of a definitive peak at that same elution time for background air. There is a higher-than-average SF_6 background concentration on the Oak Ridge Reservation, probably related to decades of uranium enrichment activities in which it was reported that SF_6 was used "by the train-car load." By contrast, no PFT peaks were apparent in background samples. Care has been taken to do all standard preparation under the hood, and standards from the pure PFT solutions are prepared in a different lab to prevent contamination of lab air.

Sensitivity: The "standards" used in these preliminary studies were made from 1% (by weight) aqueous solutions of the three PFTs that were created approximately 3 years ago. Because it is anticipated that there has been some loss of tracer over time, the concentrations have to be treated as nominally 1%. Thus, they are not truly standards in an absolute sense. Actual quantitative determination of the minimum detection limit and calibration of the GC response will require making new standards from fresh PFT sources, standards identical to those that will be used in the actual laboratory and field tracer experiments. This is necessary because in addition to the potential loss of tracer from solution over time, the tracers will have only 90–92% purity. The impurities are likely to include trace amounts of other PFTs. These trace amounts are not a problem for the kind of tracer separation experiments that are planned, as long as the impurities are identified and calibration curves are determined for the actual source being used for the experiments.

However, the results from analysis of the 1% solutions can be used to estimate the sensitivity of the analytical method, assuming no loss of tracer over time. The analytical method will be at least as sensitive as the estimate, and more sensitive if loss has occurred. Assuming no loss of tracer from solution over time and total volatilization into the headspace, tracer masses were determined for PMCP from the analyses of single and multitracer standards. For the various single and multi-tracer mixtures, 5, 10, or 15 ml of 1% solution was added to the EPA vials to create the standards. Headspace volumes varied from 25 to 35 ml. For each case, the total mass and concentration of PMCP in the headspace was calculated, and the mass injected was determined. The injection mass ranged from 5.5 to 30 ng, and a graph of GC response versus mass is shown in **Figure 32.**

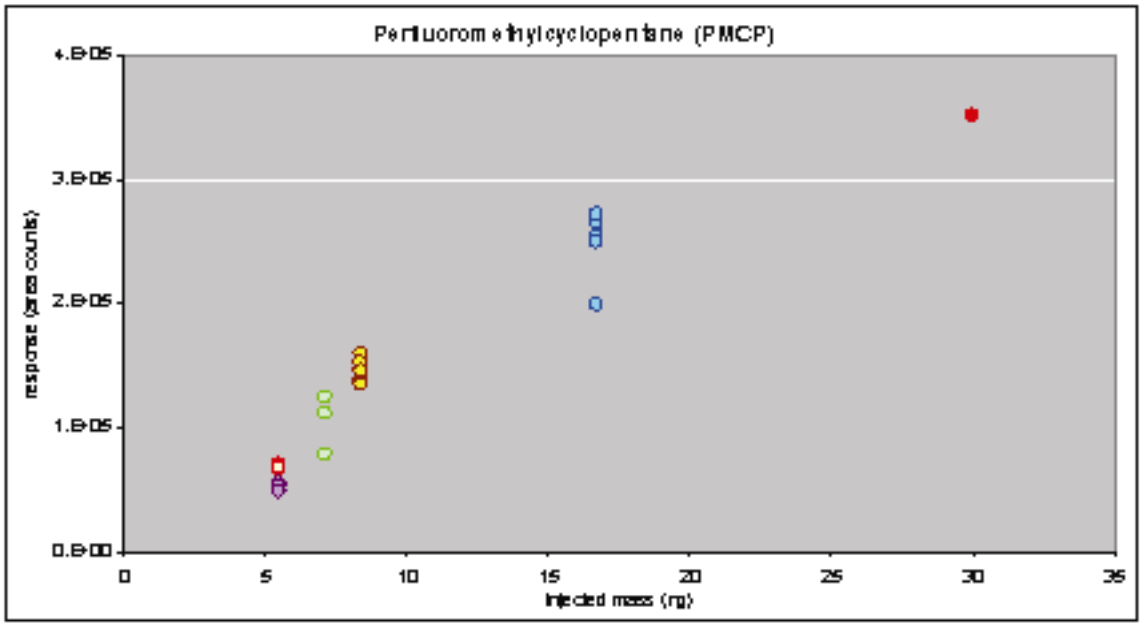

Figure 32. GC responses for various masses of PMCP injected. Mass calculations are based on an assumed 1% PFT concentration (by wt. %) for the tracer solutions.

The data show significant variation in the GC response for a given injection mass. However, these data include all the errors incurred from lack of sufficient equilibration, as previously described. With revised analytical procedures that allow sufficient time and the preparation of fresh standards

for each set of measurements, it is anticipated that this variability will be significantly reduced. For the purposes of estimating the detection sensitivity, **Figure 32** represents a "worst case" scenario. A 2-3 order of magnitude drop in concentration will still be detectable by the GC method adopted (down to roughly 1,000 counts). An additional 2-3 orders of magnitude improvement can be obtained by increasing the injection volume from 5 μl to 5 ml. Any correction due to loss of tracer from the 1% solutions will only increase the lower-limit sensitivity. Thus, the detection of 10^{-12} to 10^{-15} g of tracer is very likely. New PFT samples have been obtained from a supplier in the UK (F2 Chemicals, Ltd.), and experiments are under way to quantify the GC response, determine calibration curves for each of the tracers, and identify spurious peaks associated with impurities.

Work Next Quarter

During the next quarter efforts will focus on five main areas:

1. Continue chemical and isotopic assessment of the gases sampled on 10/20/02 at Lost Hills, California.
2. Complete noble gas isotope analyses on samples from the Lost Hills system.
3. Complete He porosimetry and single PFT tracer flow experiments using the Ottawa sand.
4. Initiate He porosimetry and single PFT tracer experiments on Frio sand.
5. Initiate preliminary modeling (with LBNL) of tracer behavior determined from dynamic flow experiments.

Subtask B-3A: The Frio Pilot Test-Monitoring with Introduced Tracers and Stable Isotopes

Goals

To provide tracer and stable isotope methods that will help quantify the fate and transport of CO_2 injected into the subsurface at the Frio, Texas, site (Task E). The resulting data will be used to calibrate and validate predictive models used for (1) estimating CO_2 residence time, reservoir storage capacity, and storage mechanisms; (2) testing injection scenarios for process optimization; and (3) assessing the potential leakage of CO_2 from the reservoir.

Previous Main Achievement

- Preliminary mineralogical characterization of the sandstone sample of the Frio Formation was completed.

Accomplishments This Quarter

- Preliminary gas chemistry and isotope analysis of CO_2 from the BP Hydrogen 1 plant, Texas City, Texas, was conducted in support of permitting documentation for CO_2 injection into the Frio formation.

Progress This Quarter

To use both the gas chemistry and stable isotopes of carbon and oxygen as potential tracers for CO_2 injection during the NETL-sponsored Frio injection test, a representative sample of the initial CO_2 injectate must be obtained. Upon the recommendation of Charles Christopher (Upstream Technology Group, BP America Inc), arrangements were made to collect a sample of "dry" CO_2 from the BP Hydrogen Unit 1 plant in Texas City, Texas, into an evacuated 1-liter gas lecture cylinder. Optimization Engineer Jonathan Sterne of BP coordinated the sample collection. The chemistry and stable isotopes of carbon and oxygen of this gas were determined using standard gas chromatographic and mass spectrometric methods (see sample preparation and analytical procedures described below). The results of these analyses are given in **Table 2**. The accepted unit of isotope ratio measurements is the delta value (δ), given in per mil (‰). The δ-value is defined as

$$\delta \text{ in } ‰ = [(R_{[sample]} - R_{[standard]}) / R_{[standard]}] \times 1000$$

where R represents the isotope ratio, either $^{13}C/^{12}C$ or $^{18}O/^{16}O$. The internationally accepted standards are PDB (a fossilized belemnite from the Peedee formation, South Carolina) for carbon and VSMOW (Vienna Standard Mean Ocean Water) for oxygen.

Table 2. Gas chemistry (mol %) and stable carbon and oxygen isotopes (in ‰) of gas collected from BP's Hydrogen Unit 1 plant, Texas City, Texas

O_2 + Ar	N_2	CO_2	CH_4	$\delta^{13}C$ CO_2	$\delta^{18}O$ CO_2
0.01	0.07	99.9	0.02	-38.84	+11.81

Based on our analyses, we observe that the gas is composed almost exclusively of CO_2. Only minor amounts of oxygen, argon, and nitrogen were detected. The only other appreciable carbon-bearing gas measured was methane at 0.02 mol %. For mol % values ranging from about 0.01 to 1, the error is on the order of 5%; for abundant species like CO_2, the error is approximately 2%. Trace quantities at the ppm level of higher hydrocarbons, ethane through hexane, were detected in scans of the mass spectra, but not quantified because of their very low abundance. The isotope values are comparable to other analyses reported for CO_2 rich gases derived from chemical processing and related anthropogenic sources. The amount of methane present was not sufficient to yield a reliable carbon isotope value.

Work Next Quarter

Our efforts in the next quarter will focus on three main areas:

1. Complete adsorption/desorption experiments on the Frio samples as a function of PCO_2 (up to 20 bars) and temperatures up to 80°C.
2. Characterize the chemistry and stable isotopes of fluid, gas. and solid Frio samples obtained from 60°C batch experiment currently in progress.
3. Assist in drafting the permitting documents needed for the Frio injection test.

Task C: Enhance and Compare Simulations Models

Subtask C-1: Enhancement of Numerical Simulators for Greenhouse Gas Sequestration in Deep, Unmineable Coal Seams

Goals

To improve simulation models for capacity and performance assessment of CO_2 sequestration in deep, unmineable coal seams.

Previous Main Achievements

- Reservoir simulator-code-comparison studies are underway, providing a mechanism for establishing current capabilities, needs for improvement, and confidence in simulation models. Based on this comparison study, the newly improved numerical simulators—CMG's GEM, ARI's COMET3, CSIRO/TNO's SIMED II, BP's GCOMP and Imperial College's METSIM2—have been validated.

- Comparisons for the first two sets of simple numerical simulation problems in Part I with pure CO_2 injection and in Part II with flue gas injection have been completed. The current participants are the aforementioned six companies. The results have been posted in the ARC's password protected website: http://www.arc.ab.ca/extranet/ecbm/

Accomplishments This Quarter

- Comparison for the Problem Sets 3 and 4 in Part III with more complex problems is ongoing. Results from CMG's GEM, CSIRO/TNO's SIMED II, ARI's COMET3, GeoQuest's ECLIPSE, BP's GCOMP, and Imperial College's METSIM2 have been documented.

- Field data obtained from two single-well, micropilot tests with pure CO_2 injection and flue gas injection, conducted by the Alberta Research Council (ARC) at the Fenn Big Valley site, Alberta, Canada, have been released to five participants (i.e., TNO, BP, CMG, ARI, and Imperial College) for history matching (i.e., Problem Set 5). This release of data provides an opportunity to validate new developments in simulation models in a realistic field situation.

Progress This Quarter

Newly collected numerical results from CMG's GEM and ARI's COMET2 for Problem Set 3 in Part III (More Complex Problems) have been documented. Problem Set 3 enhances Problem Set 2 (i.e., a five-spot CO_2 injection/production process) by taking into account the effect of gas desorption time (or gas diffusion) between the coal matrix and the natural fracture system. Comparison results among GEM, SIMED II, METSIM2, and COMET with a gas desorption time of 77.2 days are shown in **Figures 33 and 34** for CH_4 production rates and CH_4/CO_2 production composition, respectively. Discrepancies among the results during the early period of CO_2 injection are being investigated.

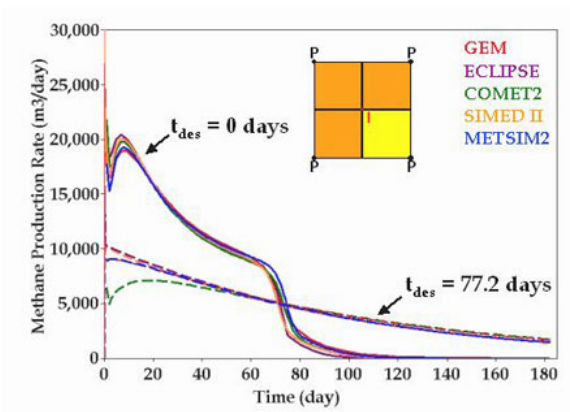

Figure 33. Problem Set 3: CH_4 Production Rates

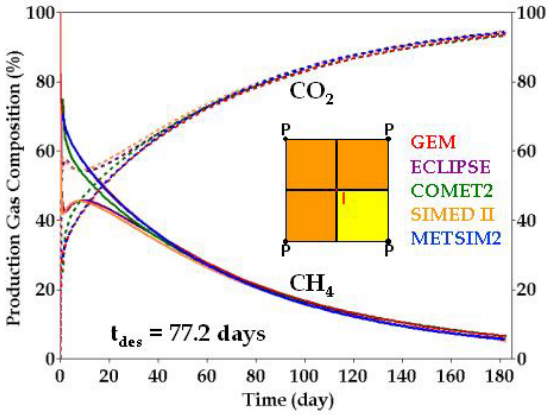

Figure 34. Problem Set 3: CH_4 and CO_2 Production Composition

Figure 35 shows CO_2 distribution as CO_2 mole fraction in the gas phase of the fracture system for Problem Set 3 with a gas desorption time of 77.2 days.

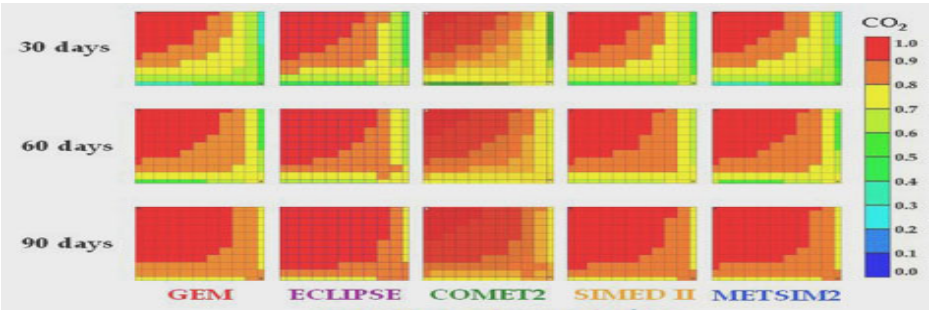

Figure 35. **Problem Set 3: CO_2 Gas Mole Fraction in Coal Fracture System**

Newly collected numerical results from ARI's COMET2 for Problem Set 4 in Part III (More Complex Problems) have been documented. Problem Set 4 enhances Problem Set 2 (i.e., a five-

spot CO_2 injection/production process) by taking into account the effect of natural fracture permeability as a function of natural fracture pressure (see **Figure 36**). Comparison results among GEM, COMET2, SIMED II, GCOMP, and METSIM2 are shown in **Figure 37** for CH_4 production rates. In general, agreement among the results is good.

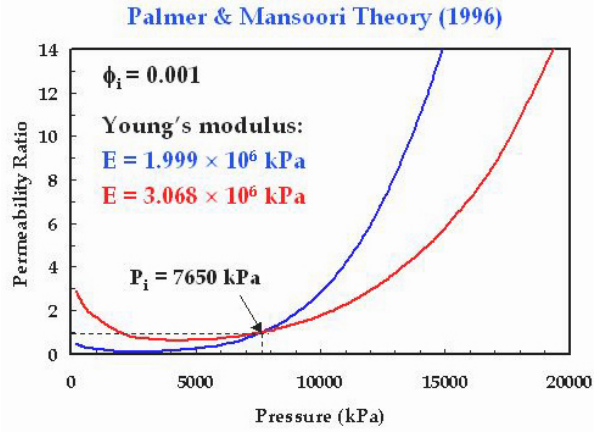

Figure 36. Problem Set 4: Effect of Pressure-Dependent Permeability

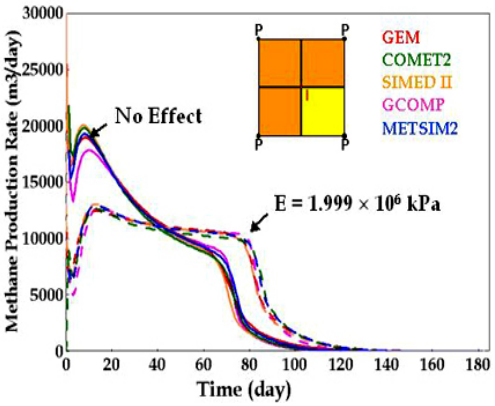

Figure 37. Problem Set 4: CH_4 Production Rates

Figure 38 shows CO_2 distribution as CO_2 mole fraction in the gas phase in the fracture system for Problem Set 4.

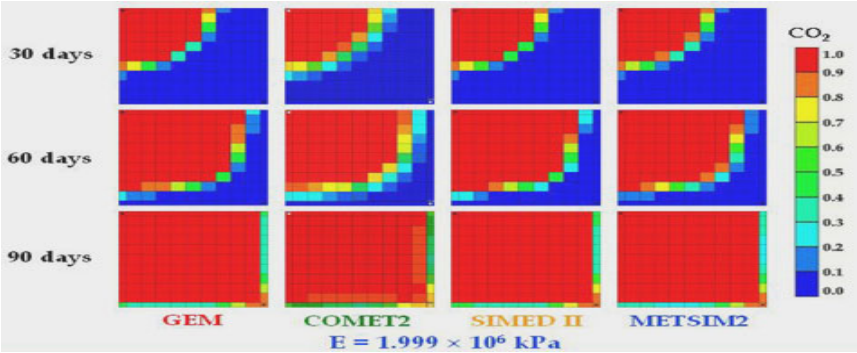

Figure 38. Problem Set 4: CO_2 Gas Mole Fraction in Coal Fracture System

Work Next Quarter

ARC will continue to collect and document numerical results from potential new participants such as Shell's MoReS for problem sets in Parts I–III. These results will be posted in the ARC website, together with the published results from the previous participants.

With the cooperation of CMG, ARC will conduct a history match of the field data using the numerical simulator, GEM. Under an agreement between ARC and CMG, a new algorithm, developed by ARC to describe the permeability variation of coal during CO_2 and flue gas injection, is being incorporated into GEM.

Subtask C-2: Intercomparison of Reservoir Simulation Models for Oil, Gas, and Brine Formulations

Goals

To stimulate the development of models for predicting, optimizing, and verifying CO_2 sequestration in oil, gas, and brine formations. The approach involves: (1) developing a set of benchmark

problems; (2) soliciting and obtaining solutions for these problems; (3) holding workshops that involve industrial, academic, and laboratory researchers; and (4) publishing results.

Previous Main Achievements

- A first workshop on the code intercomparison project was held at Berkeley Lab on October 29–30, 2001, with the first modeling results by different groups showing reasonable agreement for most problems.

Accomplishments This Quarter

- Further simulations were performed for the intercomparison test problems.
- Additional results were obtained from participating groups.
- Comparisons of results were made, and individual groups were contacted in an effort to reconcile certain differences.
- Write-ups for individual test problems were written and compiled.
- A final report on the code intercomparison study was completed in draft form.

Progress this Quarter

We performed additional simulations for the intercomparison test problems, and we received additional results from participating groups. Results from different groups were compared, agreements as well as some discrepancies were noted, and several groups were contacted in an effort to reconcile differences. Writeups summarizing intercomparisons were produced for individual test problems. Two papers on the code intercomparison study were presented at the GHGT-6 conference in Kyoto/Japan. A final report on the code intercomparison was completed, pending further revisions after internal review.

We also wrote a more detailed report with LBNL results on the saline aquifer test problems.

We received review comments on a paper entitled "Numerical Modeling of Aquifer Disposal of CO_2" that had been submitted for possible publication in the *SPE Journal* of the Society of Petroleum Engineers. The review comments were favorable; we made the minor revisions suggested by the reviewers and the revised paper was accepted for publication.

Work Next Quarter

We will make final revisions on the two reports from the code intercomparison study. This will complete Subtask C-2.

Task D: Improve the Methodology and Information for Capacity Assessment

Goals

To improve the methodology and information available for assessing the capacity of oil, gas, brine, and unmineable coal formations; and to provide realistic and quantitative data for construction of computer simulations that will provide more reliable sequestration-capacity estimates.

Previous Main Achievements

- A new definition of formation capacity, incorporating intrinsic rock capacity, geometric capacity, formation heterogeneity, and rock porosity, was developed for use in assessing sequestration capacity.

Accomplishments This Quarter

- Performed modeling studies of the Frio pilot CO_2 injection experiment (Task E), using a heterogeneous model of the South Liberty site, focusing on the impact of the characteristic curves used (in particular the residual gas saturation, S_{gr}).

- Additional calculations of the interactions between porosity and residual saturation were carried out.

Progress This Quarter

New modeling studies of the South Liberty field, location of the Frio pilot CO_2 injection experiment, were conducted. Earlier pilot-site modeling studies are described in the three previous quarterly reports. The present studies consider CO_2 injection into the C sand (which is 12 m thick and lies at a depth of about 1,500 m), using the same "Version 0" model described previously. A perspective view and a plan view of the model are shown in **Figure 39**.

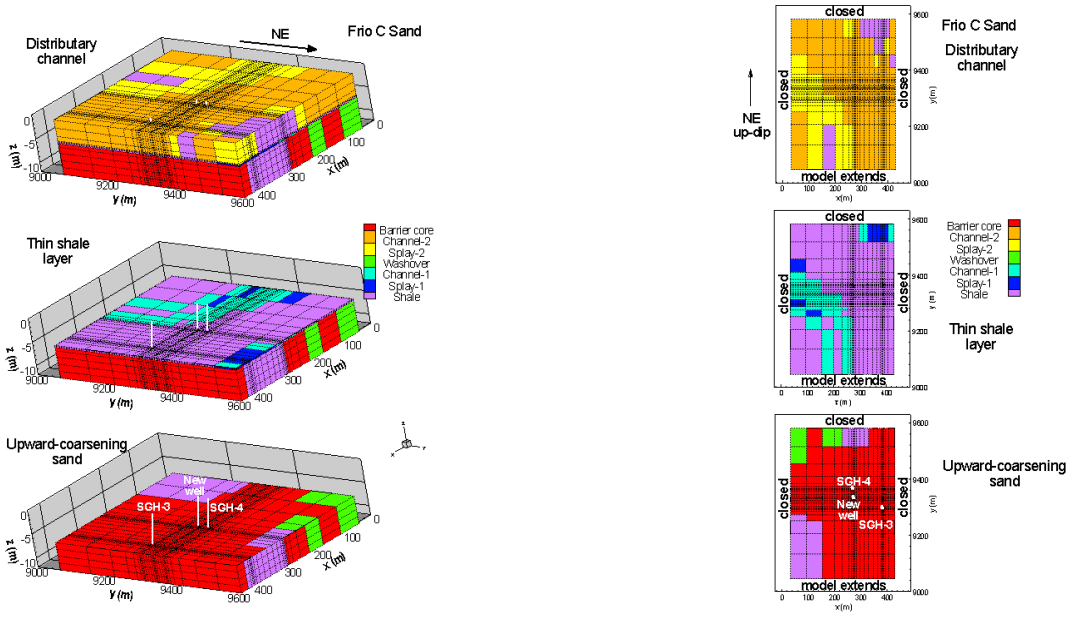

Figure 39. The Version 0 model of the Frio C sand, showing a perspective view and a plan view of each depositional setting

We modeled injection of supercritical CO_2 into the new well (**Figure 39**) at a rate of 250 T/d (2.89 kg/s) for a period of 20 days. The injection interval is the 6 m thick sand beneath the thin shale layer shown in **Figure 39**. Two cases are considered. One case uses generic characteristic curves in which the relative permeability function has a residual gas saturation S_{gr} = 0.05. The other case uses a relative permeability function with S_{gr} = 0.30, which is believed to be typical of the Frio sands. **Figures 40 and 41** show snapshots of the injected CO_2 plume during and after the 20-day injection period for the generic and Frio-like characteristic curves, respectively.

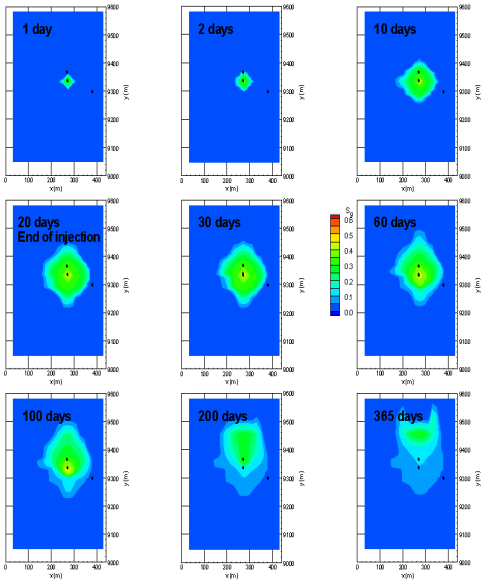

Figure 40. Snapshots of the CO_2 plume during and after the 20-day injection period, using generic characteristic curves with S_{gr} = 0.05

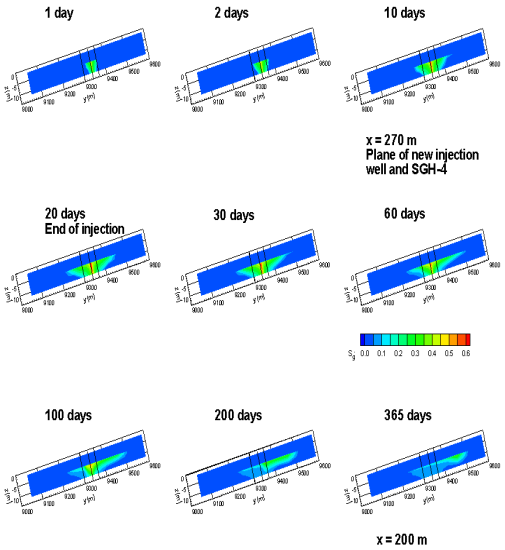

Figure 41. Snapshots of the CO_2 plume during and after the 20-day injection period, using Frio-like characteristic curves with S_{gr} = 0.30

Comparing **Figures 40 and 41**, we find that during the injection period, gas saturation S_g in the injected CO_2 plume is much larger when S_{gr} is larger; thus, the CO_2 plume is more compact. During the postinjection rest period, buoyancy flow has a much smaller effect on the CO_2 plume with larger S_{gr}.

Figures 42, 43, and 44 show the gas- and liquid-phase velocity fields for the two cases at 1, 20, and 365 days, respectively. The figures show plan views of the top model layer of the lower C sand: the whole compartment and a zoom-in of the area around the new injection well and monitoring well SGH-4. The +y direction is up-dip (15° dip). For the zoom-in view, the model grid is also shown. For the velocity plots, the tail of the velocity vectors identifies their location. The length and color of the vector indicates the magnitude of the velocity. (The scale for **Figure 44** is different, since velocities are much lower after injection ends.) Note that during injection (**Figures 42 and 43**) for larger S_{gr}, gas velocities are smaller because with a compact CO_2 plume, gas does not have to travel very far. More liquid is displaced by the higher Sg plume, so liquid velocities are larger.

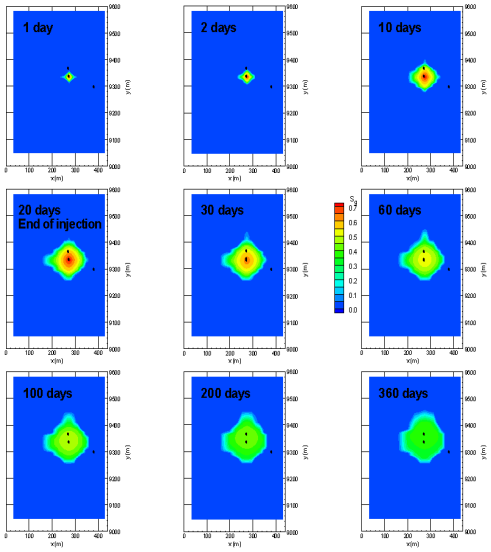

Figure 42. Gas saturation, gas velocity, and liquid velocity fields after 1 day of injection for (a) generic characteristic curves with S_{gr} = 0.05 and (b) Frio-like characteristic curves with S_{gr} = 0.30

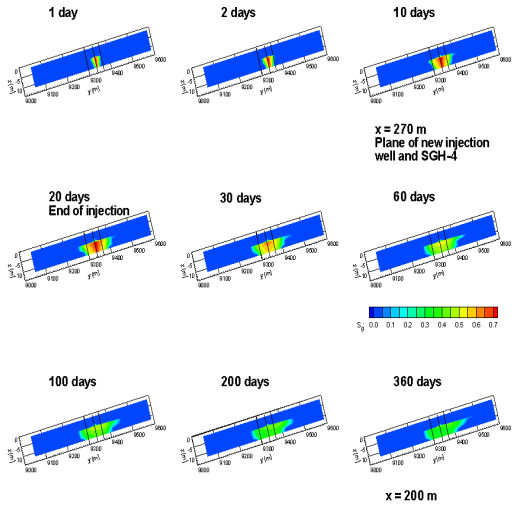

Figure 43. Gas saturation, gas velocity, and liquid velocity fields at the end of the 20-day injection period for (a) generic characteristic curves with S_{gr} = 0.05 and (b) Frio-like characteristic curves with S_{gr} = 0.30

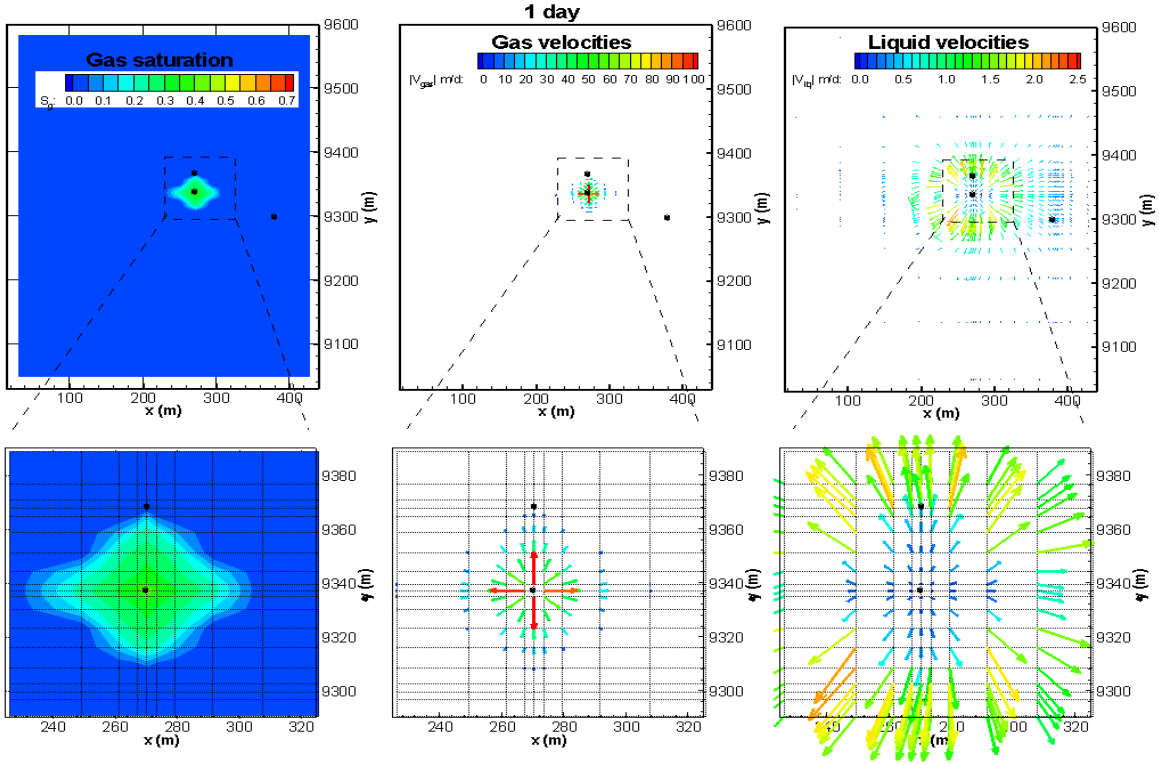

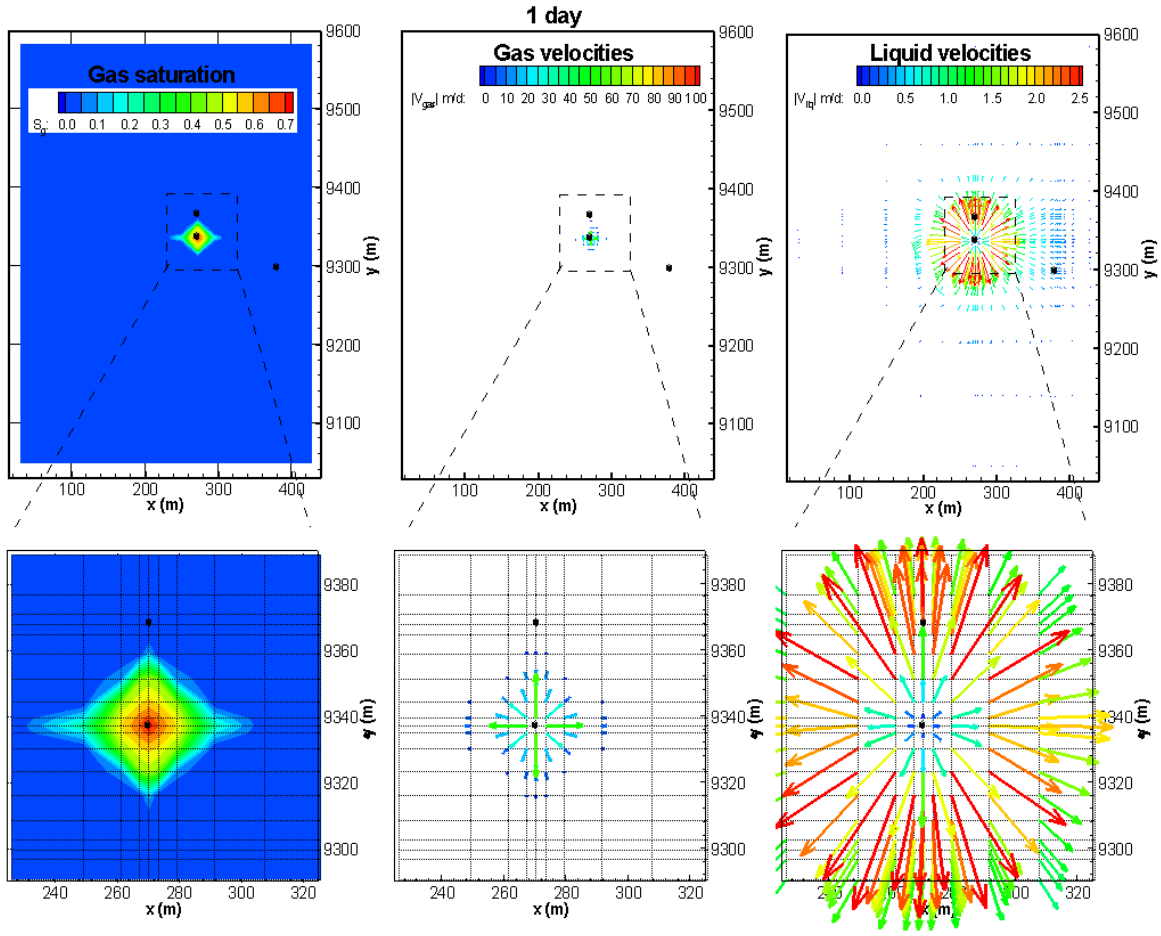

Figure 44. Gas saturation, gas velocity, and liquid velocity fields one year after the start of injection for (a) generic characteristic curves with S_{gr} = 0.05 and (b) Frio-like characteristic curves with S_{gr} = 0.30

Figures 39–44 suggest that the residual gas saturation has a strong impact on the evolution of the CO_2 plume. A higher residual saturation results in larger gas saturations in the injected plume, resulting in a more efficient use of the subsurface volume available for sequestration.

As another activity under this subtask, laboratory analysis results from the Felix Jackson core obtained from Chambers County were interpreted in context with other residual saturation data (**Figure 45**). Residual saturation is the fraction of an immiscible fluid that cannot be drained from a two-phase mixture in a porous medium as a result of capillary forces in pores. Applying the residual saturation to the porosity available (**Figure 46**) determines a bulk volume of CO_2 that will be trapped by residual saturation.

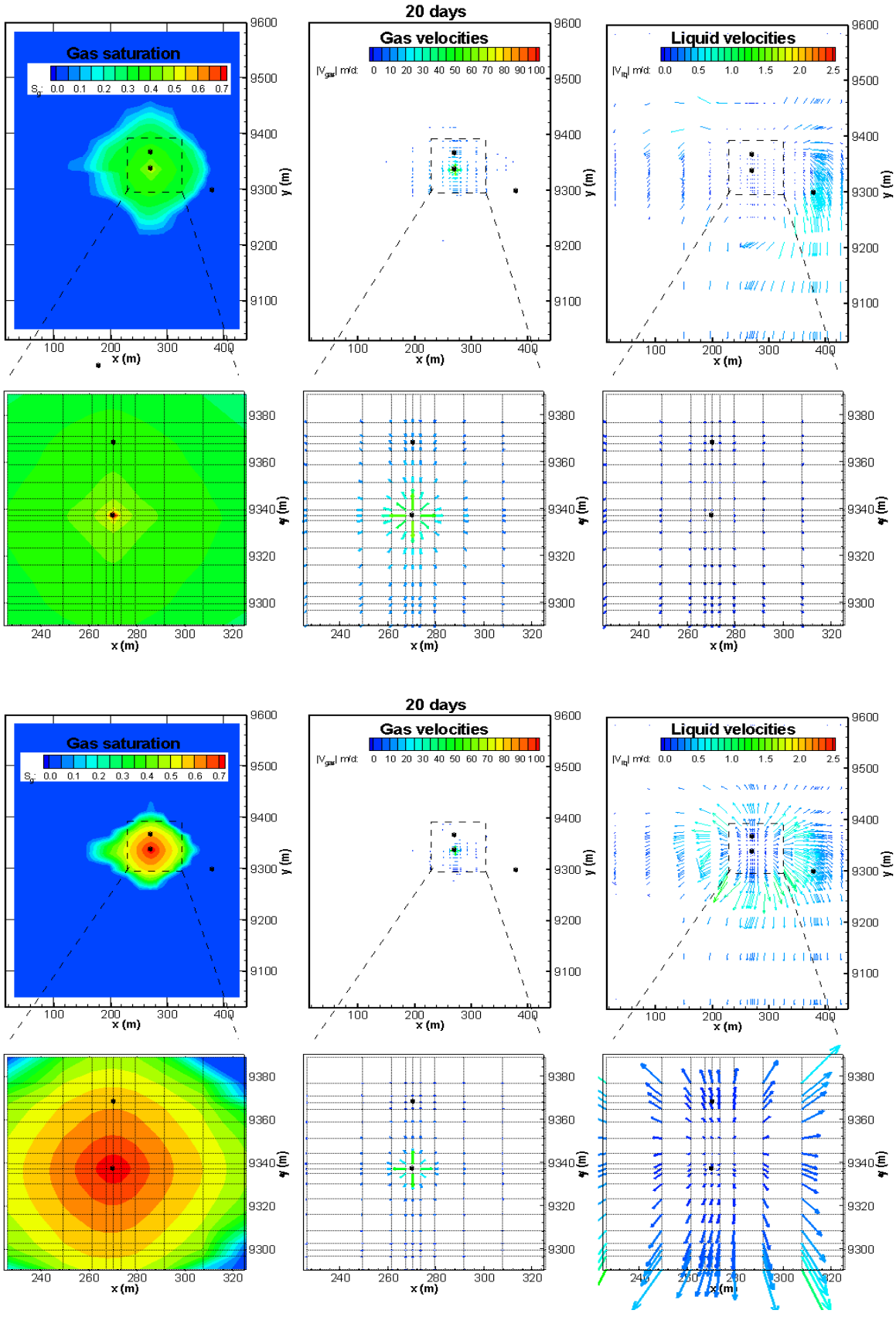

Figure 45. Comparison of Frio residual gas saturation with published data

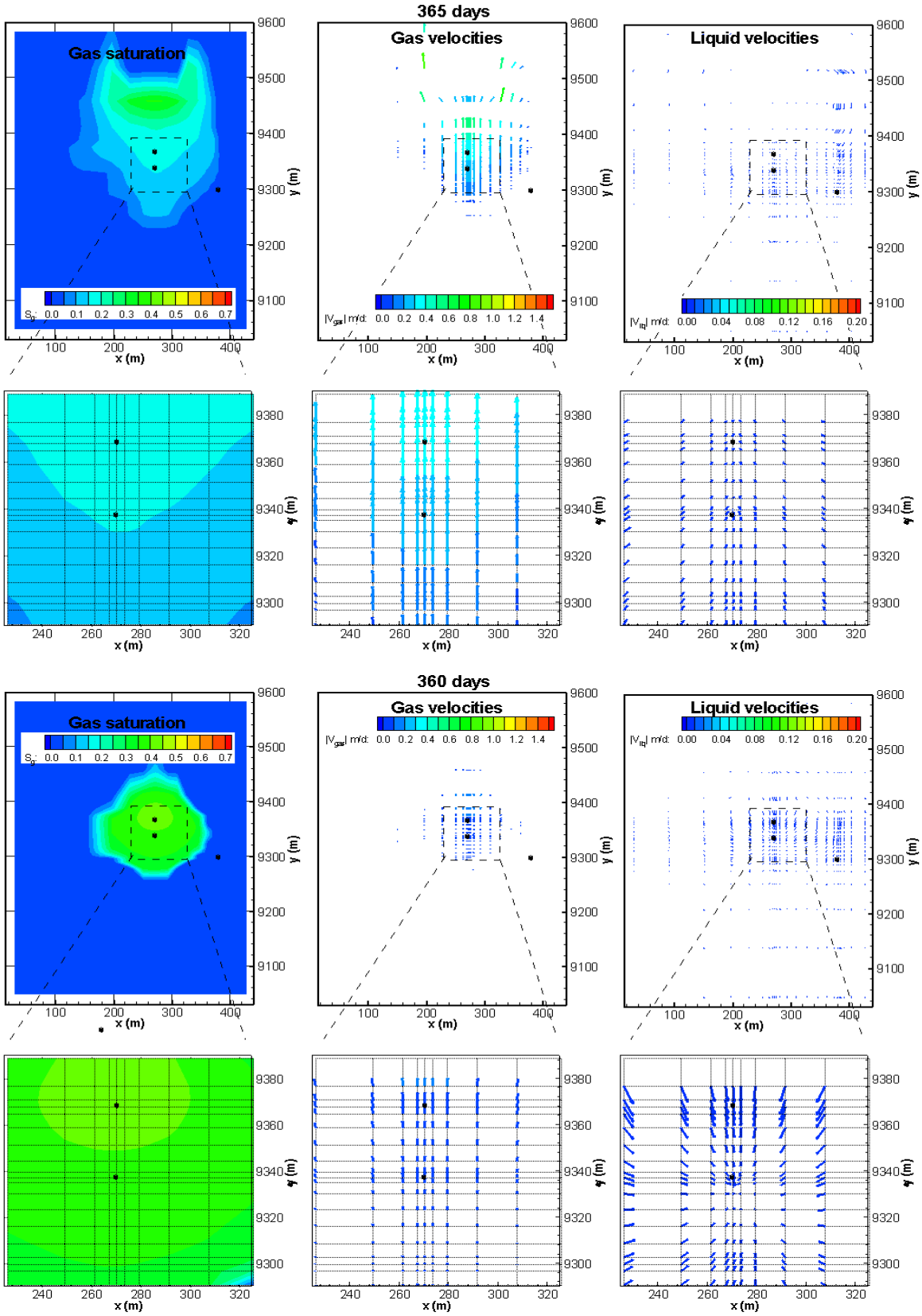

Figure 46. Residual phase sequestration optimization curve

Data collection is under way to create a statistically based geologic model for the pathways that would be occupied by CO_2 from a location in the upper Texas coast. Combining the residual saturation trapping with structural trapping along flow paths will be used to calculate the length of a plume resulting from a given injection scenario and volumes stored along these plumes.

Work Next Quarter

Further simulations will replicate more closely the currently envisioned pilot-site test conditions:

- The South Liberty geologic model developed at BEG is currently being adapted to work with TOUGH2. This work is nearly complete. The next stage will be to refine the computational grid around the locations of the proposed new injection well and the existing monitoring well SGH-4. These wells will only be about 30 m apart, which is comparable to the present grid spacing. Such grid spacing may be used to examine the long-term evolution of the injected CO_2 plume over the entire fault block, but it does not allow adequate resolution for simulation of well tests or breakthrough of the injected CO_2 at the nearby monitoring well.

- We will consider various means to broaden the scope of the model simulations to include wellbore processes, enabling prediction of wellhead conditions. If the connection between reservoir conditions and wellhead conditions can be made with confidence, then monitoring at the wellhead, which is easier and cheaper than monitoring downhole, can be used far more productively. Wellbore processes are expected to involve a complex combination of fluid flow and heat transport, including phase changes. Experience with geothermal wellbore simulators will be tapped.

- We will complete data collection from Geomap structural maps for the Houston area and will compile statistics to describe typical volumes within fault closure and quantify the pathways of spillover from the structures. These data will be used to develop a statistically based geologic model for the pathways that would be occupied by a large plume of CO_2 during the injection and post-injection phases of sequestration, to assess trapping and sequestration effectiveness. These data should provide input for further modeling efforts to assess capacity.

Task E: Frio Brine Pilot Project

Goals

To perform numerical simulations and conduct field experiments at the Frio Brine Pilot site, near Houston, Texas, that:

- Demonstrate that CO_2 can be injected into a saline formation without adverse health, safety, or environmental effects.

- Determine the subsurface location and distribution of the cloud of injected CO_2.

- Demonstrate understanding of conceptual models.

- Develop the experience necessary for the success of large-scale CO_2 injection experiments.

Note: This task does not include work being done by the Texas Bureau of Economic Geology under the project “Optimal Geological Environments for Carbon Dioxide Disposal in Brine Formations (Saline Aquifers) in the United States,” funded under a separate contract.

Previous Main Achievements

- A planning workshop was held at BEG (Austin, Texas) on July 8–9, 2002 to explore the interrelationships among the modeling and monitoring techniques proposed by the GEO-SEQ

team for conducting the Frio Brine Pilot Test. A time line and a more detailed plan for implementation of modeling and monitoring techniques were developed.

- A proposal to construct a new injection well instead of retrofitting a 50-year-old oil well was prepared. The new well would be closer to the monitoring well and directly down dip. Less CO_2 and a shorter injection period will be required to achieve breakthrough in the monitoring well.

Accomplishments This Quarter

- Permit preparation is nearing completion, with substantive input from GEO-SEQ team.

- More detailed plans have been created to integrate the various GEO-SEQ experiments with the well design and test schedule

- Initial contacts with stakeholders—including the community, regulators, industry, and NGS— have been made to lay groundwork for the permitting process, using outreach materials developed by GEO-SEQ.

Progress this Quarter

During this period, the activities were focused on the preparation of the permitting documents needed for the injection experiment. We must complete the federal NEPA process and obtain a Class 5 experimental injection well permit from the State of Texas prior to field mobilization. BEG and subcontractor Sandia Technologies are preparing the NEPA document and Class 5 permit as part of the Frio pilot project, with a substantive contribution by the GEO-SEQ team. This contribution includes numerous TOUGH2 model runs, reactive-transport modeling, and laboratory analyses of CO_2 from the source to be used for injection, as well as core to provide high-quality data to support the permits.

In addition, we have met with community members near the pilot site, independent operators, utilities, and representatives of NGOs to provide information about the project prior to the formal permitting and NEPA review process. Outreach materials developed as part of GEO-SEQ continue to be used, especially in nontechnical discussions.

A deterministic model of the injection interval and overlying monitoring horizon, based on the 3-D seismic and reservoir characterization, has been completed and formatted for input into the simulation code TOUGH2.

Work Next Quarter

Next quarter we will complete the report to support the Class 5 permit application to the Texas Commission on Environmental Quality and the NEPA EA. The GEO-SEQ contributions to these tasks will include building the next version of the TOUGH2 model. We will continue coordination to assure that research opportunities employing the skills the GEO-SEQ team is maximized in the experiment. We continue to have discussion with other potential industry participants in the experiment.
.
We will continue to work with stakeholders in the Houston area to prepare for public hearings to be held on these documents in the future, including field-testing the outreach materials in a school near the injection site. Moreover, a planning meeting is scheduled to be held in Houston on December 6, to further coordinate the planning of the injection test, focusing on the geophysical measurements.